HAL
open science

Analytical and numerical simplified modeling of a single-lap joint

Tuan Hung Nguyen, Philippe Le Grognec

To cite this version:

Tuan Hung Nguyen, Philippe Le Grognec. Analytical and numerical simplified modeling of a single-lap joint. International Journal of Adhesion and Adhesives, 2021, 108, pp.102827. 10.1016/j.ijadhadh.2021.102827 . hal-03212389

HAL Id: hal-03212389

https://ensta-bretagne.hal.science/hal-03212389

Submitted on 31 May 2021

HAL is a multi-disciplinary open access archive for the deposit and dissemination of scientific research documents, whether they are published or not. The documents may come from teaching and research institutions in France or abroad, or from public or private research centers.

L'archive ouverte pluridisciplinaire **HAL**, est destinée au dépôt et à la diffusion de documents scientifiques de niveau recherche, publiés ou non, émanant des établissements d'enseignement et de recherche français ou étrangers, des laboratoires publics ou privés.

Analytical and numerical simplified modeling of a single-lap joint

Tuan Hung Nguyen[a], Philippe Le Grognec[a,*]

[a] *ENSTA Bretagne, UMR CNRS 6027, IRDL, F-29200 Brest, France*

Abstract

This paper is devoted to the theoretical modeling of the mechanical response of bonded structures and particularly focuses on the single-lap joint which corresponds to the simplest and most fundamental bonding configuration. Such a geometry brings into play all the features of any bonded assembly in terms of mechanical response (stress/strain heterogeneities, singularities, adhesion at the interfaces, ...). It can especially be used to characterize the mechanical behavior of new adhesives within an assembly. In all cases, an accurate description of the stress/strain distribution (specifically in the adhesive layer) is required both for the calibration of an adhesive behavior and for dimensioning purposes. Accordingly, the present study aims at developing a specific 1D enriched finite element devoted to the numerical modeling of single-lap joints, especially of the overlap region. First, analytical solutions for a single-lap joint under tensile forces are investigated in the framework of elasticity. They are particularly based on the choice of a 2D representation of the adhesive layer with polynomial displacement fields in terms of the thickness coordinate. Such a preliminary study allows one to identify optimally the appropriate kinematics for each layer (adhesive but also substrates) and highlights the importance of non-linear terms in the polynomial expressions of both longitudinal and transverse displacements within the adhesive. A three-layer finite element model is then formulated for the overlap region, based on the retained kinematics, and involving an elastoplastic constitutive law for the adhesive material. The numerical integration through the adhesive thickness and the assembly of the three layers lead to the definition of a very low-cost 1D finite element, which provides nevertheless a complete and accurate description of the stress fields, especially within the adhesive layer. This new finite element (used simultaneously with a more classical beam finite element for the unbonded parts of the adherends) is finally validated by comparison with 2D reference results computed using Abaqus software.

Keywords: Single-lap joint, Enriched kinematics, Analytical modeling, 1D finite element, Elastoplasticity

*Corresponding author.
Email address: philippe.le_grognec@ensta-bretagne.fr (Philippe Le Grognec)

1. Introduction

The use of adhesive bonding for assembling structures brings many advantages when compared to other conventional methods such as welding or riveting: it enables a simple and efficient assembly procedure while avoiding any weight increase and limiting material damage. Therefore, structural bonding is increasingly used in many industrial applications, especially in the automotive, naval and aeronautical fields. The single-lap joint (SLJ) is certainly the most inherently fundamental bonded assembly. It represents the simplest bonding configuration and, at the same time, brings into play all the features of any bonded assembly in terms of mechanical response (stress/strain heterogeneities, singularities, adhesion at the interfaces, ...). This configuration can especially be used to characterize the mechanical behavior of new adhesives within an assembly, under various loadings and environmental factors such as humidity or temperature. In all cases, an accurate description of the stress/strain distribution (specifically in the adhesive layer) is required whether for the calibration of the adhesive behavior or for dimensioning purposes.

Therefore, SLJs have been the subject of many studies during the last decades, which most often aim at identifying failure criteria for assemblies, based on more or less accurate stress estimations. For about eighty years, numerous analytical and numerical models characterized by different levels of approximation have been defined in the literature. Analytical models are generally limited to simple configurations and include strong assumptions, such as an elastic behavior for both adhesive and substrates. Most of them are based on Volkersen's pioneering works [1] in which the adhesive layer is represented as a simple interface undergoing a non-uniform shear distribution along the length (with higher values at both ends), between two rigid bars only deforming in tension. Then, Goland and Reissner [2] considered the possible rotation of the adherends and introduced the so-called edge moment factors related to the bending-tension coupling so as to take into account the loading eccentricity. More recently, their model was extended by Mortensen and Thomsen [3]. These authors represented the adhesive layer as a combination of shear and tension/compression spring distributions and went further by analyzing the mechanical behavior of unbalanced SLJs, also including an inelastic constitutive behavior for the adhesive layer. Besides, Stein et al. [4] relied on the same kinematics in order to derive analytical solutions for functionally graded adhesive SLJs. In all the above-mentioned models (and many others), the adhesive layer is supposed to be one-dimensional, so that the stress-free condition at its ends is not respected and the evolution of stresses through the adhesive thickness cannot be captured [5]. To overcome these limitations, quasi-2D and 2D models have been developed. Early on, Allman [6] assumed a non constant peel stress along the thickness of the adhesive layer. Later, Zhao et al. [7] derived closed-form expressions of stresses in adherends and adhesive, based on 2D elastic stress-strain constitutive relations, and assumed that the peel stress varied linearly and the shear stress remained constant throughout the adhesive thickness. However, in both previous works, the longitudinal normal stress is totally neglected. Jiang et al. [8] thoroughly investigated the mechanical response of SLJs, describing the

adhesive and adherends as three distinct layers separated by flexible interfaces. In their study, they combined the use of Euler-Bernoulli/Timoshenko beams and the 2D elasticity theory, involving thus the three stress components (shear, peel and longitudinal stresses) which were supposed to vary along the thickness of the adhesive layer. Some of these authors [9, 10] further analyzed the case of unbalanced composite SLJs and derived new expressions for the stress fields and edge moment factors, in the context of large deformations.

Alternatively, owing to the numerous limitations of analytical models, many numerical models have also been proposed for the analysis of SLJs. Most of numerical studies are based on 2D/3D standard finite element models, which represent the SLJs in an explicit manner. For instance, Cognard et al. [11] analyzed the influence of various geometries of adhesive joints and corresponding edge effects on the stress concentrations in SLJs for optimization purposes. On another note, Gonçalves et al. [12] developed a 3D model of a SLJ, involving specific interface elements of zero thickness between the adherend and adhesive layers. Such models are intended to capture at best the stress distributions within the adhesive layer, but they quickly become far too time-consuming, especially when inverse identification is needed. The only way to circumvent the computation cost of such 2D/3D models is to make use of simplified numerical approaches. Several authors have already proposed some specific finite element formulations devoted to the analysis of stresses in the adhesive layer of SLJs. As a pioneering numerical work on this subject, one can cite Lin and Lin [13], who developed a simplified beam-like finite element formulation for any SLJ configuration (with possibly non identical adherends), where the longitudinal and transverse displacements are supposed to vary linearly through the adhesive thickness and the shear stress is constant accordingly (the longitudinal stress being neglected in the adhesive layer). Later on, Tong and Sun [14] investigated the mechanical behavior of a bonded patch on a curved 3D structure. In their formulation, the structure and the patch are modeled using a first-order thick shell theory, encompassing thus the transverse shear effects. Furthermore, only the out-of-plane (peel and shear) stresses are considered in the adhesive layer and they are assumed to be constant across the adhesive thickness.

One idea is to develop macro-elements with embedded analytical solutions and thus the concept of exact stiffness matrix, allowing for a mesh-independent analysis (using only one such element for the entire overlap region). In this sense, Paroissien et al. [15] developed a 1D-bar and 1D-beam simplified model, in which the adhesive mechanical response is represented by distributions of shear and/or transverse springs. An elastoplastic adhesive material behavior is also introduced in these models, keeping the same previous formulations. In a similar way, Stapleton et al. [16] proposed an enriched macro-element based on the same beam theory for the adherends and equivalent spring distributions for the adhesive layer, so as to analyze the progressive failure of bonded joints. Some of these authors [17] extended the model so as to investigate the mechanical behavior of functionally graded adhesives. More recently, in order to better capture non-linear effects due to the constitutive behavior or during cracking, they proposed the use of (i) adaptive shape functions to comply with the case of geometric and/or material non-linearities, and (ii) an internal mesh

adaptation so as to discretize the macro-element consistently with the partially cracked geometry [18]. In such models, the longitudinal stress is not included, and the shear and peel stresses are constant through the adhesive thickness (they are determined by the relative horizontal and vertical displacements of upper and lower adherend/adhesive interfaces, respectively). Indeed, the formulation of the enhanced element is compelled by the need to obtain an analytical solution of the problem, and more enriched kinematics are not eligible for such macro-elements. Moreover, the solution obtained in the adhesive layer depends on the particular geometry of the problem in hand and could not be easily extrapolated to other configurations.

The present study aims at developing new original solutions for the mechanical analysis of SLJs. The starting point is to enrich the kinematics within the adhesive layer so as to describe not only the shear and peel stresses, but also the longitudinal one, and their variation along both the length and the thickness of the adhesive joint. While the substrates are classically represented by Timoshenko beams, the adhesive zone is thus defined here as a 2D continuous medium with a polynomial dependence of the displacement fields with respect to the thickness coordinate. Unlike most previous models in the literature, such a model is supposed to describe in an integrated manner the local stress fields which may all be useful for the definition of any failure criterion, among other things. First, several analytical solutions are derived for a SLJ under tension in the context of linear elasticity, and compared with each other in order to emphasize the significant influence of non-linear terms in the kinematics on stress distributions. Then, a 1D three-layer enriched finite element is developed, which is built by assembling the previous models identified for the three layers and based on the optimal choice of polynomial orders for the description of the adhesive joint. An elastoplastic constitutive behavior is also considered for the adhesive material, with the von Mises criterion and an isotropic hardening. Finally, an original finite element program is elaborated, coupling the use of this specific element for the overlap region and classical beam elements for the remaining parts of the SLJ. All the present analytical and numerical solutions are compared to reference 2D numerical results obtained through classical finite element computations using Abaqus software, for validation purposes.

2. Analytical modeling of a single-lap joint

2.1. Problem definition

Let us consider a SLJ made of two substrates separated (and perfectly bonded) by an adhesive layer in the overlap area. The adherends are strictly identical, so that the problem is symmetric with respect to the center of the adhesive zone. A 2D representation of the SLJ (in the xy-plane) is retained, assuming a uniform depth t (in the z-direction). The length of the overlap region (along the x-axis) is $2L_a$, whereas the remaining length of each substrate is denoted by L_s (the origin $x = 0$ lies in the middle of the adhesive joint, for the sake of symmetry). The thicknesses of the adhesive layer and the two adherends (along the y-direction) are respectively $2h_a$ and $2h_s$ (see Figure 1).

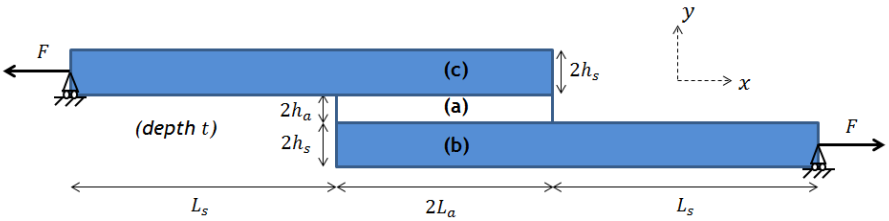

Figure 1: Two-dimensional representation of the single-lap joint

Both adhesive and substrates are assumed to be made of homogeneous, isotropic and linearly elastic materials, with Young's moduli E_i and Poisson's ratios ν_i ($i = a$ or s depending on whether adhesive or substrates are concerned). The adhesive layer is modeled as a 2D continuous solid satisfying the plane stress hypothesis. Consequently, the reduced moduli $\lambda'_a (= \frac{2\lambda_a \mu_a}{\lambda_a + 2\mu_a})$ and μ_a will be used in the subsequent analysis (where λ_a and μ_a are the Lamé constants related to E_a and ν_a by the standard relations $\lambda_a = \frac{E_a \nu_a}{(1+\nu_a)(1-2\nu_a)}$ and $\mu_a = \frac{E_a}{2(1+\nu_a)}$). Conversely, the adherends are supposed to behave like Timoshenko beams, since transverse shear effects may be non negligible in practice (Tsai et al. [19] particularly showed the importance of taking into consideration shear deformations in the adherends so as to properly describe the shear distribution in the adhesive). Owing to these kinematic hypotheses, only the Young's modulus E_s and the shear modulus $G_s = \frac{E_s}{2(1+\nu_s)}$ will be involved subsequently. Only small displacements and strains are considered throughout the paper.

2.2. Theoretical formulation

In the sequel, the static response of the SLJ problem will be classically solved by means of the virtual work principle, which generally writes:

$$\forall\ \delta\mathbf{u}_a, \delta\mathbf{u}_b, \delta\mathbf{u}_c \quad \text{(KA)}, \qquad \delta\mathcal{W}_{int} + \delta\mathcal{W}_{ext} = 0 \tag{1}$$

where $\delta\mathbf{u}_a$, $\delta\mathbf{u}_b$ and $\delta\mathbf{u}_c$ can be considered as kinematically admissible test functions or, more physically, as the virtual variations of the unknown displacement fields $\mathbf{u}_a$, and $\mathbf{u}_b$ and $\mathbf{u}_c$, in the adhesive layer and adherends, respectively.

On one side, both substrates are represented by Timoshenko beams. As far as the bending problem in the xy-plane is concerned, the Timoshenko kinematics is defined by two scalar displacement fields $u_i(x)$ and $v_i(x)$, respectively the longitudinal and transverse displacements of the centroid axis of the beam, and the rotation of its cross-section $\theta_i(x)$ about the z-axis (for $i = b$ or c, depending on the adherend considered). The general displacement field of a current point of a substrate writes then in the orthonormal basis $(\mathbf{e}_x, \mathbf{e}_y)$:

$$\mathbf{u}_i(x,y) = \left| \begin{array}{l} u_i(x) - y\theta_i(x) \\ v_i(x) \end{array} \right. \tag{2}$$

where y denotes the through-thickness position with respect to the centroid axis of the considered beam.

As a consequence, the strain and stress tensors, respectively denoted by $\boldsymbol{\varepsilon}_i$ and $\boldsymbol{\sigma}_i$ for each adherend $i = b, c$, take the following form (in Voigt notation):

$$\boldsymbol{\varepsilon}_i = \left\{ \begin{array}{c} \varepsilon^i_{xx} \\ \varepsilon^i_{yy} \\ 2\varepsilon^i_{xy} \end{array} \right\} = \left\{ \begin{array}{c} u_{i,x} - y\theta_{i,x} \\ 0 \\ v_{i,x} - \theta_i \end{array} \right\}$$
$$\boldsymbol{\sigma}_i = \left\{ \begin{array}{c} \sigma^i_{xx} \\ \sigma^i_{yy} \\ \sigma^i_{xy} \end{array} \right\} = \left\{ \begin{array}{c} E_s(u_{i,x} - y\theta_{i,x}) \\ 0 \\ G_s(v_{i,x} - \theta_i) \end{array} \right\} \tag{3}$$

On the other side, the displacement field in the adhesive layer is defined through polynomial series in terms of y-coordinate and takes thus the general following form in the orthonormal basis $(\mathbf{e}_x, \mathbf{e}_y)$:

$$\mathbf{u}_a(x, y) = \left| \begin{array}{l} \sum_{i=0}^{n} u_i(x)\ y^i \\ \sum_{j=0}^{p} v_j(x)\ y^j \end{array} \right. \tag{4}$$

Several cases (couples of values of integers n and p) were investigated in practice. Only two cases are discussed in this paper for conciseness purposes. The linear case ($n = p = 1$) is presented below, whereas the main expressions for the quadratic case ($n = p = 2$) are reported in Appendix A. Therefore, considering $n = p = 1$ in Equation (4), the longitudinal and transverse displacement components simply become:

$$\mathbf{u}_a(x, y) = \left| \begin{array}{l} u_0(x) + u_1(x)\ y \\ v_0(x) + v_1(x)\ y \end{array} \right. \tag{5}$$

The plane stress hypothesis is adopted in the subsequent analytical developments, which is supposed to reproduce at best the 3D behavior of a SLJ with relatively small lateral dimensions. The strain and stress tensors in the adhesive layer can then be deduced as follows, involving the reduced moduli defined above:

$$\boldsymbol{\varepsilon}_a = \left\{ \begin{array}{c} \varepsilon^a_{xx} \\ \varepsilon^a_{yy} \\ 2\varepsilon^a_{xy} \end{array} \right\} = \left\{ \begin{array}{c} u_{0,x} + u_{1,x}\, y \\ v_1 \\ u_1 + v_{0,x} + v_{1,x}\, y \end{array} \right\}$$
$$\boldsymbol{\sigma}_a = \left\{ \begin{array}{c} \sigma^a_{xx} \\ \sigma^a_{yy} \\ \sigma^a_{xy} \end{array} \right\} = \left\{ \begin{array}{c} (\lambda'_a + 2\mu_a)(u_{0,x} + u_{1,x}\, y) + \lambda'_a v_1 \\ \lambda'_a(u_{0,x} + u_{1,x}\, y) + (\lambda'_a + 2\mu_a)v_1 \\ \mu_a(u_1 + v_{0,x} + v_{1,x}\, y) \end{array} \right\} \tag{6}$$

The strains and stresses in Equations (3) and (6) allow one to express the internal virtual work of Equation (1):

$$\delta\mathcal{W}_{int} = -\sum_{i=a,b,c} \int_{\Omega_i} \delta\boldsymbol{\varepsilon}_i^T \boldsymbol{\sigma}_i \mathrm{d}\Omega \tag{7}$$

where Ω_a, Ω_b and Ω_c represent the reference volumes of the adhesive layer and the two substrates, respectively.

Besides, the SLJ is submitted to two symmetric tensile forces F at the ends of each substrate, as seen in Figure 1. The virtual work of these external forces limits itself to the following expression:

$$\delta\mathcal{W}_{ext} = -F\delta u_c(-L_s - L_a) + F\delta u_b(L_a + L_s) \tag{8}$$

After integration through the thickness of each layer, the virtual work principle (1) takes the following integral form:

$$\begin{aligned}
&\forall \delta u_b, \delta v_b, \delta\theta_b, \delta u_c, \delta v_c, \delta\theta_c, \delta u_0, \delta u_1, \delta v_0, \delta v_1, \\
&\int_{-L_s-L_a}^{L_a} \left[2E_s h_s u_{c,x}\,\delta u_{c,x} + \tfrac{2E_s h_s^3}{3}\theta_{c,x}\,\delta\theta_{c,x} + 2kG_s h_s(v_{c,x}\,\delta v_{c,x} + \theta_c\delta\theta_c - v_{c,x}\,\delta\theta_c - \theta_c\delta v_{c,x})\right] t\mathrm{d}x \\
&+ \int_{-L_a}^{L_a} \left[(\lambda_a' + 2\mu_a)(2h_a u_{0,x}\,\delta u_{0,x} + \tfrac{2h_a^3}{3}u_{1,x}\,\delta u_{1,x}) + \lambda_a'(2h_a v_1\delta u_{0,x} + 2h_a u_{0,x}\,\delta v_1) + 2(\lambda_a' + 2\mu_a)h_a v_1\delta v_1\right. \\
&\left. + \mu_a(2h_a u_1\delta u_1 + 2h_a u_1\delta v_{0,x} + 2h_a v_{0,x}\,\delta u_1 + 2h_a v_{0,x}\,\delta v_{0,x} + \tfrac{2h_a^3}{3}v_{1,x}\,\delta v_{1,x})\right] t\mathrm{d}x \\
&+ \int_{-L_a}^{L_a+L_s} \left[2E_s h_s u_{b,x}\,\delta u_{b,x} + \tfrac{2E_s h_s^3}{3}\theta_{b,x}\,\delta\theta_{b,x} + 2kG_s h_s(v_{b,x}\,\delta v_{b,x} + \theta_b\delta\theta_b - v_{b,x}\,\delta\theta_b - \theta_b\delta v_{b,x})\right] t\mathrm{d}x \\
&+ F\delta u_c(-L_s - L_a) - F\delta u_b(L_a + L_s) = 0
\end{aligned} \tag{9}$$

At this stage, continuity conditions must be specified for the displacement fields at the interfaces between the adhesive layer and the two substrates, namely:

$$\forall x \in]-L_a, L_a[, \qquad \begin{aligned} \mathbf{u}_b(x, h_s) &= \mathbf{u}_a(x, -h_a) \\ \mathbf{u}_c(x, -h_s) &= \mathbf{u}_a(x, h_a) \end{aligned} \tag{10}$$

Inserting Equations (2) and (5) in Equation (10) allows one to derive the following expressions for u_b, v_b, u_c and v_c:

$$\forall x \in]-L_a, L_a[, \qquad \begin{aligned} u_b &= h_s\theta_b + u_0 - h_a u_1 \\ v_b &= v_0 - h_a v_1 \\ u_c &= -h_s\theta_c + u_0 + h_a u_1 \\ v_c &= v_0 + h_a v_1 \end{aligned} \tag{11}$$

Accordingly, in Equation (9), these four displacement components as well as the corresponding virtual quantities are replaced by the previous expressions in terms of the other displacement components u_0, u_1, v_0, v_1, θ_b and θ_c.

Finally, the following set of differential equations of equilibrium can be deduced after integration by parts of Equation (9) with respect to x:

- $\forall x \in]-L_s - L_a, -L_a[$:

$$\begin{aligned} &2E_s h_s u_{c,xx}^l = 0 \\ &2kG_s h_s(v_{c,xx}^l - \theta_{c,x}^l) = 0 \\ &\tfrac{2E_s h_s^3}{3}\theta_{c,xx}^l + 2kG_s h_s(v_{c,x}^l - \theta_c^l) = 0 \end{aligned} \tag{12}$$

- $\forall x \in]-L_a, L_a[$:

$$\begin{aligned}
&\tfrac{2E_s h_s^3}{3}\theta_{b,xx} + 2E_s h_s^2(h_s\theta_{b,xx} + u_{0,xx} - h_a u_{1,xx}) + 2kG_s h_s(-\theta_b + v_{0,x} - h_a v_{1,x}) = 0\\
&\tfrac{2E_s h_s^3}{3}\theta_{c,xx} - 2E_s h_s^2(-h_s\theta_{c,xx} + u_{0,xx} + h_a u_{1,xx}) + 2kG_s h_s(-\theta_c + v_{0,x} + h_a v_{1,x}) = 0\\
&2(\lambda'_a + 2\mu_a)h_a u_{0,xx} + 2\lambda'_a h_a v_{1,x} + 2E_s h_s(h_s\theta_{b,xx} - h_s\theta_{c,xx} + 2u_{0,xx}) = 0\\
&(\lambda'_a + 2\mu_a)\tfrac{2h_a^3}{3}u_{1,xx} - \mu_a(2h_a u_1 + 2h_a v_{0,x}) + 2E_s h_s h_a(-h_s\theta_{b,xx} - h_s\theta_{c,xx} + 2h_a u_{1,xx}) = 0\\
&\mu_a(2h_a u_{1,x} + 2h_a v_{0,xx}) + 2kG_s h_s(-\theta_{b,x} - \theta_{c,x} + 2v_{0,xx}) = 0\\
&2\lambda'_a h_a u_{0,x} + 2(\lambda'_a + 2\mu_a)h_a v_1 - \mu_a\tfrac{2h_a^3}{3}v_{1,xx} - 2kG_s h_s h_a(\theta_{b,x} - \theta_{c,x} + 2h_a v_{1,xx}) = 0
\end{aligned} \tag{13}$$

- $\forall x \in]L_a, L_a + L_s[$:

$$\begin{aligned}
&2E_s h_s u^r_{b,xx} = 0\\
&2kG_s h_s(v^r_{b,xx} - \theta^r_{b,x}) = 0\\
&\tfrac{2E_s h_s^3}{3}\theta^r_{b,xx} + 2kG_s h_s(v^r_{b,x} - \theta^r_b) = 0
\end{aligned} \tag{14}$$

Equations (12) and (14) refer to the left part of adherend c and right part of adherend b, respectively, and superscripts $\bullet^l$ and $\bullet^r$ have been added to the associated displacement components. Furthermore, Equation (13) involves the three layers within the overlap region.

In the subsequent analysis, Equations (12-14) will be solved together with the following boundary/continuity conditions. Hereinafter, some kinematic (displacement) conditions are introduced when appropriate, and the remaining natural (stress) conditions derive automatically from the previous integrations by parts.

First, the adherends are supposed to be simply-supported at both ends of the SLJ. It leads to the following classical boundary conditions for beams:

- For $x = -L_s - L_a$:

$$\begin{aligned}
&2E_s h_s t u^l_{c,x} - F = 0 && \text{(axial force)}\\
&v^l_c = 0 && \text{(no vertical displacement)}\\
&\tfrac{2E_s h_s^3}{3}\theta^l_{c,x} = 0 && \text{(no bending moment)}
\end{aligned} \tag{15}$$

- For $x = L_a + L_s$:

$$\begin{aligned}
&2E_s h_s t u^r_{b,x} - F = 0 && \text{(axial force)}\\
&v^r_b = 0 && \text{(no vertical displacement)}\\
&\tfrac{2E_s h_s^3}{3}\theta^r_{b,x} = 0 && \text{(no bending moment)}
\end{aligned} \tag{16}$$

Next, at both connections between the substrates and the overlap region, the continuity of displacements must be satisfied, which can be expressed as follows:

- For $x = -L_a$:

$$\begin{aligned} u_c^l &= -h_s\theta_c + u_0 + h_a u_1 \\ v_c^l &= v_0 + h_a v_1 \\ \theta_c^l &= \theta_c \end{aligned} \tag{17}$$

- For $x = L_a$:

$$\begin{aligned} u_b^r &= h_s\theta_b + u_0 - h_a u_1 \\ v_b^r &= v_0 - h_a v_1 \\ \theta_b^r &= \theta_b \end{aligned} \tag{18}$$

The remaining natural conditions stand for the continuity of resultant stresses along the substrates and the free boundaries of the adhesive layer at both sides:

- For $x = -L_a$:

$$\begin{aligned} &\tfrac{2E_s h_s^3}{3}(\theta_{c,x}^l - 4\theta_{c,x}) + 2E_s h_s^2(-u_{c,x}^l + u_{0,x} + h_a u_{1,x}) = 0 \\ &\tfrac{8E_s h_s^3}{3}\theta_{b,x} + 2E_s h_s^2(u_{0,x} - h_a u_{1,x}) = 0 \\ &2(\lambda_a' + 2\mu_a)h_a u_{0,x} + 2\lambda_a' h_a v_1 + 2E_s h_s(h_s\theta_{b,x} - h_s\theta_{c,x} - u_{c,x}^l + 2u_{0,x}) = 0 \\ &(\lambda_a' + 2\mu_a)\tfrac{2h_a^3}{3}u_{1,x} + 2E_s h_s h_a(-h_s\theta_{b,x} - h_s\theta_{c,x} - u_{c,x}^l + 2h_a u_{1,x}) = 0 \\ &\mu_a(2h_a u_1 + 2h_a v_{0,x}) + 2kG_s h_s(-\theta_b - \theta_c + \theta_c^l - v_{c,x}^l + 2v_{0,x}) = 0 \\ &\mu_a\tfrac{2h_a^3}{3}v_{1,x} + 2kG_s h_s h_a(\theta_b - \theta_c + \theta_c^l - v_{c,x}^l + 2h_a v_{1,x}) = 0 \end{aligned} \tag{19}$$

- For $x = L_a$:

$$\begin{aligned} &\tfrac{2E_s h_s^3}{3}(4\theta_{b,x} - \theta_{b,x}^r) + 2E_s h_s^2(-u_{b,x}^r + u_{0,x} - h_a u_{1,x}) = 0 \\ &\tfrac{8E_s h_s^3}{3}\theta_{c,x} - 2E_s h_s^2(u_{0,x} + h_a u_{1,x}) = 0 \\ &2(\lambda_a' + 2\mu_a)h_a u_{0,x} + 2\lambda_a' h_a v_1 + 2E_s h_s(h_s\theta_{b,x} - h_s\theta_{c,x} - u_{b,x}^r + 2u_{0,x}) = 0 \\ &(\lambda_a' + 2\mu_a)\tfrac{2h_a^3}{3}u_{1,x} + 2E_s h_s h_a(-h_s\theta_{b,x} - h_s\theta_{c,x} + u_{b,x}^r + 2h_a u_{1,x}) = 0 \\ &\mu_a(2h_a u_1 + 2h_a v_{0,x}) + 2kG_s h_s(-\theta_b - \theta_c + \theta_b^r - v_{b,x}^r + 2v_{0,x}) = 0 \\ &\mu_a\tfrac{2h_a^3}{3}v_{1,x} + 2kG_s h_s h_a(\theta_b - \theta_c - \theta_b^r + v_{b,x}^r + 2h_a v_{1,x}) = 0 \end{aligned} \tag{20}$$

2.3. Solution procedure

The differential equations above are solved sequentially in the following way. First, Equations (12) and (14) are solved for adherend c and b respectively, together with boundary conditions (15) and (16). The

solutions are as follows:

$$\begin{cases} u_c^l = \frac{F}{2E_s h_s} x - c_1 \\ v_c^l = \frac{1}{6}\left[\left(-2L_a^2 + (2x-4L_s)L_a + x^2 + 2xL_s - 2L_s^2\right)c_2 + 6c_3\right](x + L_a + L_s) \\ \theta_c^l = \frac{1}{6kG_s}\left[3kG_s\left(x(x+2L_a+2L_s)c_2 + 2c_3\right) + 2E_s h_s^2 c_2\right] \\ u_b^r = \frac{F}{2E_s h_s} x + c_1 \\ v_b^r = \frac{1}{6}\left[\left(-2L_a^2 - (2x+4L_s)L_a + x^2 - 2xL_s - 2L_s^2\right)c_2 + 6c_3\right](x - L_a - L_s) \\ \theta_b^r = \frac{1}{6kG_s}\left[3kG_s\left(x(x-2L_a-2L_s)c_2 + 2c_3\right) + 2E_s h_s^2 c_2\right] \end{cases} \tag{21}$$

Owing to the symmetry of the problem, the same three constants c_1, c_2 and c_3 have been introduced for the two substrates. These constants will be determined along with the other ones after solving the remaining differential equations.

Equation (13) can be recast so as to eliminate the rotation fields θ_b and θ_c. This gives rise to two sets of two differential equations, the first in terms of u_0 and v_1, and the second involving u_1 and v_0. The general (symmetric) solutions of these equations write:

$$\begin{cases} u_1 = k_1 + k_2 x^2 + k_3 \cosh\left(\frac{\sqrt{6kG_s\mu_a}\sqrt{(\lambda_a'+2\mu_a)h_a^3+6E_s h_s h_a^2+12E_s h_s^2 h_a+8E_s h_s^3}x}{2h_s\sqrt{E_s h_a}\sqrt{2kG_s h_s+\mu_a h_a}\sqrt{3E_s h_s+2(\lambda_a'+2\mu_a)h_a}}\right) \\ v_0 = k_1' x + k_2' x^3 + k_3' \sinh\left(\frac{\sqrt{6kG_s\mu_a}\sqrt{(\lambda_a'+2\mu_a)h_a^3+6E_s h_s h_a^2+12E_s h_s^2 h_a+8E_s h_s^3}x}{2h_s\sqrt{E_s h_a}\sqrt{2kG_s h_s+\mu_a h_a}\sqrt{3E_s h_s+2(\lambda_a'+2\mu_a)h_a}}\right) \end{cases} \tag{22}$$

and:

$$\begin{cases} u_0 = k_1'' x + k_2'' \cosh(\alpha x)\sin(\beta x) + k_3'' \sinh(\alpha x)\cos(\beta x) \\ v_1 = k_1''' + k_2''' \cosh(\alpha x)\cos(\beta x) + k_3''' \sinh(\alpha x)\sin(\beta x) \end{cases} \tag{23}$$

where α and β are respectively the real and imaginary parts of:

$$\begin{aligned} \xi = \; & \left(3kG_s\mu_a(\lambda_a'+2\mu_a)h_a^3 + 6kG_sE_s\mu_a h_s h_a^2 + \left((-36kG_s+48\mu_a)\lambda_a' + 48\mu_a^2\right)E_s h_s^2 h_a + 6E_s^2(\lambda_a'+2\mu_a)h_s^3\right. \\ & -3\left(4(\lambda_a'+2\mu_a)^2 E_s^4 h_s^6 - 8E_s^3(\lambda_a'+2\mu_a)\left[kG_s\mu_a h_a + \left(-8\mu_a(\lambda_a'+\mu_a) + 6kG_s(2kG_s+\lambda_a')\right)h_s\right]\right. \\ & +4E_s^2\left[k^2G_s^2\mu_a^2 h_a^2 - kG_s\mu_a\left(20\mu_a(\lambda_a'+\mu_a) + \lambda_a'(12kG_s+7\lambda_a')\right)h_s h_a\right. \\ & -4\left(-16\mu_a^3(2\lambda_a'+\mu_a) + \mu_a^2(60k^2G_s^2 + 24kG_s\lambda_a' - 16\lambda_a'^2) + 12kG_s\lambda_a'\mu_a(5kG_s+2\lambda_a') + 3k^2G_s^2\lambda_a'^2\right)h_s^2\Big]h_s^2 \\ & +4kG_sE_s\mu_a(\lambda_a'+2\mu_a)\left(kG_s\mu_a h_a^2 - 2(3kG_s\lambda_a' + 4\mu_a(\lambda_a'+\mu_a))h_s h_a - 96kG_s(\lambda_a'+\mu_a)h_s^2\right)h_s h_a^3 \\ & \left.+k^2G_s^2\mu_a^2(\lambda_a'+2\mu_a)^2 h_a^6\right)^{\frac{1}{2}}\Big)^{\frac{1}{2}} \Big/ \left(2h_s\sqrt{E_s h_a}\sqrt{6kG_s h_s + \mu_a h_a}\sqrt{E_s h_s + 2(\lambda_a'+2\mu_a)h_a}\right) \end{aligned} \tag{24}$$

The coefficients k_i, k_i', k_i'', k_i''' $(i = 1, 2, 3)$ are constant values which can all be expressed in terms of only 6 independent parameters. Finally, when considering also the constants introduced in Equation (21), 9 unknown factors remain, which can be deduced from the conditions (17) and (19) (or (18) and (20) by symmetry) as the solution of a linear algebraic equation system.

3. Validation and discussion

3.1. Numerical simulation using Abaqus

Two-dimensional numerical finite element computations have been performed using Abaqus software, in order to compare the previous different analytical solutions to reference numerical results. For this purpose, the 2D geometry of Figure 1 is again considered. Both adhesive and substrates are represented by a 2D continuous solid satisfying the plane stress condition, according to the similar assumption made in the previous formulation. The finite element mesh is made up of 8-node quadrangular elements with reduced integration. After a few preliminary convergence analyses, the same mesh is retained for all the subsequent calculations, displaying 200 elements along the overlap length, 100 elements along the length of the remaining part of each substrate, 20 elements in the thickness of the adhesive layer and 10 elements in the thickness of each adherend. The boundary conditions are consistent with the ones described in the theoretical formulation. At both sides of the SLJ, the point figuring the end of the centroid axis of each substrate is fixed in the transverse direction so as to reflect the simple support conditions at best. Furthermore, the axial forces are uniformly distributed on the corresponding edges.

3.2. Comparison between analytical and numerical solutions

Many computations have been performed, varying the geometric and material parameters, so as to explore the relative validity of the different analytical solutions (obtained with various polynomial orders in the kinematics). The same observations have been made in all cases, particularly for a large range of thickness ratio (between adhesive and adherends) and thickness-to-length ratio (of the adhesive layer). Hence, for conciseness purposes, a single geometric and material configuration will be investigated in all the subsequent analyses, which is intended to reproduce the typical trends of such a problem. The geometric and material parameters considered are listed in Tables 1 and 2, respectively.

L_s (mm)	L_a (mm)	h_s (mm)	h_a (mm)	t (mm)
75	12.5	1	0.2	25

Table 1: Geometric parameters

E_s (MPa)	E_a (MPa)	ν_s	ν_a
210000	6500	0.3	0.36

Table 2: Material properties [20]

In the analytical formulation, a first-order shear theory is used for the description of the substrates, and a shear correction factor of 5/6 is assigned to them, as classically done for rectangular cross-sections. Finally, an arbitrary force of 5000 N is applied at both ends of the SLJ.

In Figures 2 and 3, different stress profiles are plotted along the overlap length, for validation purposes. Figure 2 displays the longitudinal (σ_{xx}), peel/transverse (σ_{yy}) and shear (σ_{xy}) stresses along the centroid axis of the adhesive layer, whereas Figure 3 plots the same stresses at the upper interface between adhesive and adherend, within the adhesive zone.

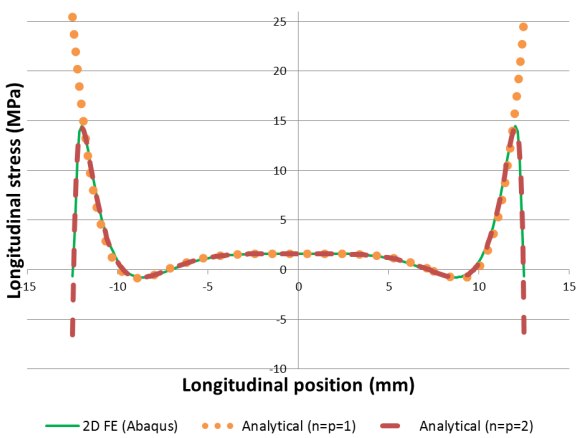

(a) Longitudinal stresses

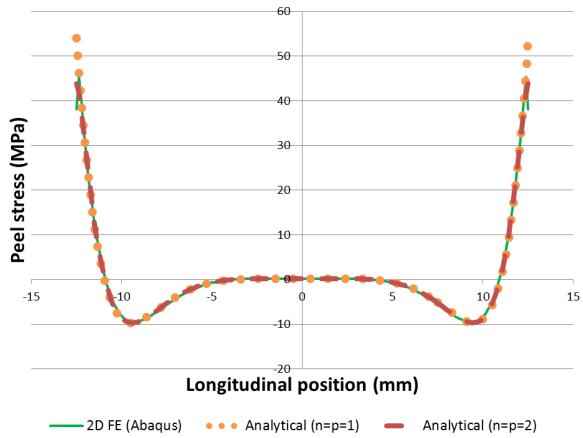

(b) Peel stresses

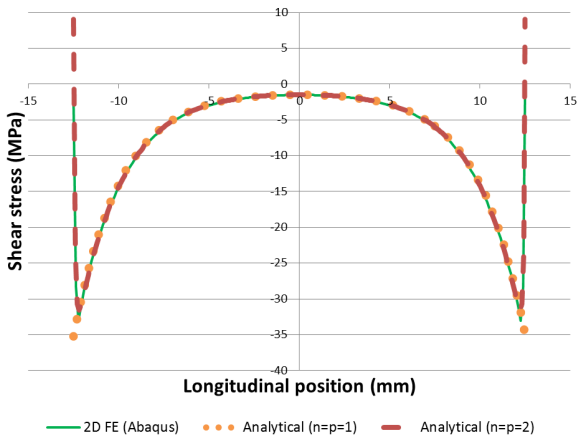

(c) Shear stresses

Figure 2: Comparison of analytical and numerical stresses along the mid-line of the adhesive layer

In each case, three curves are represented: two analytical curves with the linear ($n = p = 1$) and quadratic ($n = p = 2$) kinematics, respectively, and one numerical curve related to the 2D finite element computations.

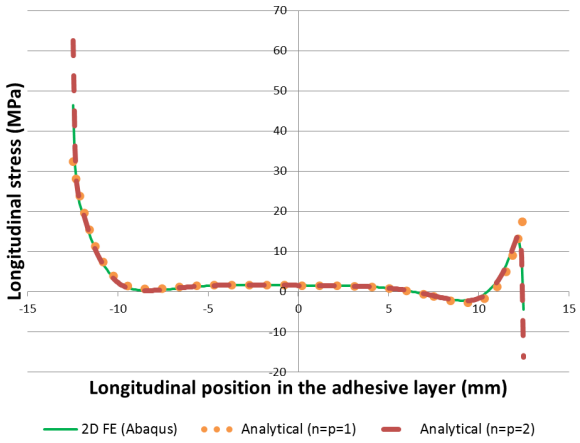

(a) Longitudinal stresses

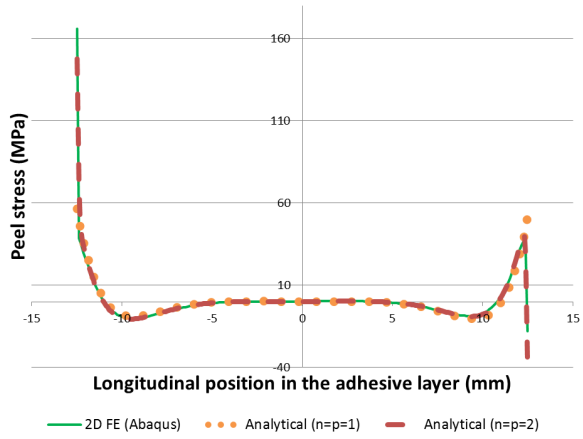

(b) Peel stresses

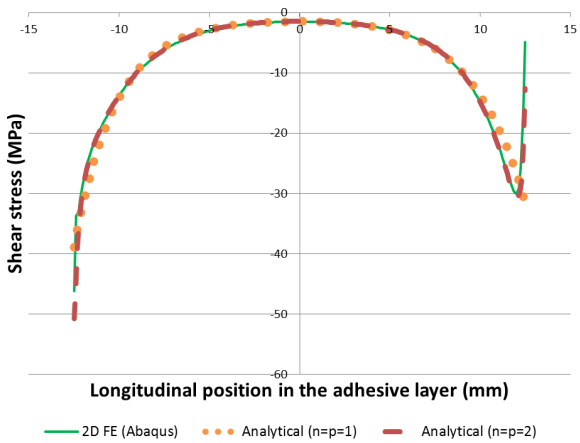

(c) Shear stresses

Figure 3: Comparison of analytical and numerical stresses along the upper interface

3.3. Analysis and discussion

In both figures 2 and 3, all the results are quite in a good agreement in a large central portion of the curves. It means that, broadly speaking, both kinematics (even the linear one) are capable to reproduce the real (2D) mechanical response of the SLJ under axial tensile forces. However, on closer inspection, one realizes that the "linear" and "quadratic" solutions really differ from each other at both ends. The curves corresponding to the quadratic model are almost similar to the numerical ones. Only slight differences appear: they are due to significant stress variations which are especially encountered near the singularity at the corner (at the left end of the upper interface), see Figure 3(b); substantial relative differences are also pointed out when stresses theoretically tend to zero (at both free ends), since in the analytical model, this boundary condition is only taken into account in an average sense (see Figure 2(a) and Figure 2(c)).

Conversely, the "linear" analytical solution does not display the same trends as in the numerical results. The strong variations at one or both ends in almost every stress profile are never observed with this simple model.

All these observations show the importance of non-linear terms in the kinematics description for dimensioning purposes. Indeed, the highest stress levels are generally encountered at the ends of the adhesive joint and the failure initiation is supposed to occur there, whatever the retained criterion. It is thus necessary to estimate accurately the stress distributions even to the extremities. In practice, a quadratic/cubic approximation (for the longitudinal/transverse displacement fields, respectively) turns out to be the best compromise concerning the choice of kinematics for the adhesive layer. In the next section, a specific three-layer 1D finite element is developed so as to deal with more complex geometric, material and/or loading configurations. It is specially based on the same polynomial kinematics in the adhesive layer as used in the previous analytical study, including a fortiori non-linear terms.

4. An enriched 1D finite element for the analysis of single-lap joints

Thereafter, the mechanical behavior of a SLJ is investigated from a numerical point of view, in order to deal more easily with other non-linear constitutive laws, various loading and boundary conditions and, in the longer term, with more general geometric configurations. For obvious efficiency purposes, it is decided to develop a 1D enriched finite element for the three-layer assembly on the basis of what was done before in the preliminary analytical study. An original "SLJ" finite element model is then built, which consists in such enriched elements together with classical beam elements for the unbonded parts of the substrates (see Figure 4).

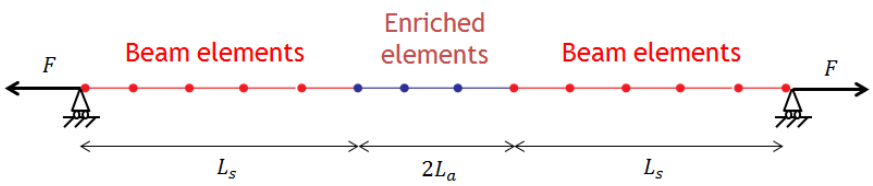

Figure 4: One-dimensional finite element model of the single-lap joint

4.1. Kinematics and constitutive laws

The same geometric and material configuration is considered, as in the previous analytical section, and the same notations are used (see Figure 1). The adherends b and c are still represented by Timoshenko beams accounting for transverse shear effects, and the associated displacement and strain fields are thus

given by Equations (2) and (3), respectively. In the general case of an isotropic linear elastic material, the stress-strain relation in the adherends can be expressed as follows:

$$\boldsymbol{\sigma}_i = \mathbf{L}_s \boldsymbol{\varepsilon}_i \qquad (i = b, c) \tag{25}$$

so as to introduce the elastic constitutive operator $\mathbf{L}_s$ for later use:

$$\mathbf{L}_s = \begin{bmatrix} E_s & 0 & 0 \\ 0 & 0 & 0 \\ 0 & 0 & G_s \end{bmatrix} \tag{26}$$

The adhesive layer a is described using enriched 2D kinematics. Both longitudinal and transverse displacement fields are represented by polynomial functions of the thickness coordinate. Thanks to the previous analysis, the optimal choice of quadratic longitudinal ($n = 2$) and cubic transverse ($p = 3$) displacements is retained, which results in a proper representation of the through-thickness distribution of strain/stress fields. The final displacement fields write then:

$$\mathbf{u}_a(x, y) = \left| \begin{array}{l} u_0(x) + u_1(x)\ y + u_2(x)\ y^2 \\ v_0(x) + v_1(x)\ y + v_2(x)\ y^2 + v_3(x)\ y^3 \end{array} \right. \tag{27}$$

From Equation (27), one can define the strain field as follows:

$$\boldsymbol{\varepsilon}_a = \left\{ \begin{array}{c} \varepsilon^a_{xx} \\ \varepsilon^a_{yy} \\ 2\varepsilon^a_{xy} \end{array} \right\} = \left\{ \begin{array}{c} u_{0,x} + u_{1,x}\, y + u_{2,x}\, y^2 \\ v_1 + 2v_2 y + 3v_3 y^2 \\ u_1 + 2u_2 y + v_{0,x} + v_{1,x}\, y + v_{2,x}\, y^2 + v_{3,x}\, y^3 \end{array} \right\} \tag{28}$$

In further numerical analyses, the adhesive material will be considered either elastic or elastoplastic. In elasticity, the stress field is expressed here through the constitutive operator $\mathbf{L}_a$, similarly to Equation (25):

$$\boldsymbol{\sigma}_a = \mathbf{L}_a \boldsymbol{\varepsilon}_a \tag{29}$$

Only the plane stress condition will be investigated below. Under such an assumption, the following expression holds for the elasticity matrix:

$$\mathbf{L}_a = \begin{bmatrix} \lambda'_a + 2\mu_a & \lambda'_a & 0 \\ \lambda'_a & \lambda'_a + 2\mu_a & 0 \\ 0 & 0 & \mu_a \end{bmatrix} \tag{30}$$

In the plastic regime, the J_2 flow theory is adopted and the plastic threshold of the adhesive material is defined by the von Mises yield function with a linear isotropic hardening. The classical expression of this criterion in a 3D framework is slightly transformed here so as to fulfill the 2D plane stress condition:

$$f(\boldsymbol{\sigma}_a, A) = \frac{1}{2}\boldsymbol{\sigma}_a^T \mathbf{P} \boldsymbol{\sigma}_a - \frac{1}{3}(\sigma^a_y + A)^2 \qquad \text{(with } A = H_a p) \tag{31}$$

where $\mathbf{P}$ is the deviatoric operator, p is the equivalent plastic strain, and σ_y^a and H_a stand for the initial yield stress and the (constant) hardening modulus of the adhesive material, respectively.

The strain vector $\boldsymbol{\varepsilon}_a$ may be split additively into its elastic and plastic parts:

$$\boldsymbol{\varepsilon}_a = \boldsymbol{\varepsilon}_a^e + \boldsymbol{\varepsilon}_a^p \tag{32}$$

Then, the associated flow rule is derived from the yield function, according to the generalized standard materials theory, giving rise to the plastic strain rate:

$$\dot{\boldsymbol{\varepsilon}}_a^p = \dot{\Lambda}\frac{\partial f}{\partial \boldsymbol{\sigma}_a} = \dot{\Lambda}\mathbf{P}\boldsymbol{\sigma}_a \tag{33}$$

where the plastic multiplier $\dot{\Lambda}$ is related to the equivalent plastic strain rate by:

$$\dot{p} = \dot{\Lambda}\sqrt{\frac{2}{3}\boldsymbol{\sigma}_a^T\mathbf{P}\boldsymbol{\sigma}_a} \tag{34}$$

The polynomial coefficients $u_0(x)$, $u_1(x)$, $u_2(x)$, $v_0(x)$, $v_1(x)$, $v_2(x)$, $v_3(x)$, together with $u_b(x)$, $u_c(x)$, $v_b(x)$, $v_c(x)$, $\theta_b(x)$, $\theta_c(x)$, are the unknowns of the problem, which only depend on the longitudinal position x and will be further discretized in order to define the desired 1D finite element model.

In the overlap region, the substrates are presumed to be perfectly bonded to the adhesive layer, what enables one to write the following relations accounting for the continuity of the displacements at the top and bottom interfaces:

- **at the upper adherend/adhesive interface:**

$$\mathbf{u}_c(x,-h_s) = \mathbf{u}_a(x,h_a) \implies \begin{cases} u_c + h_s\theta_c = u_0 + h_a u_1 + h_a^2 u_2 \\ v_c = v_0 + h_a v_1 + h_a^2 v_2 + h_a^3 v_3 \end{cases} \tag{35}$$

- **at the lower adherend/adhesive interface:**

$$\mathbf{u}_b(x,h_s) = \mathbf{u}_a(x,-h_a) \implies \begin{cases} u_b - h_s\theta_b = u_0 - h_a u_1 + h_a^2 u_2 \\ v_b = v_0 - h_a v_1 + h_a^2 v_2 - h_a^3 v_3 \end{cases} \tag{36}$$

Taking into consideration the aforementioned displacement continuity constraints, one can rewrite u_0, u_1, v_0 and v_1 in terms of the remaining variables in the following way:

$$\begin{aligned} u_0 &= \tfrac{1}{2}(u_c + u_b + h_s\theta_c - h_s\theta_b) - h_a^2 u_2 \\ u_1 &= \tfrac{1}{2h_a}(u_c - u_b + h_s\theta_c + h_s\theta_b) \\ v_0 &= \tfrac{1}{2}(v_c + v_b) - h_a^2 v_2 \\ v_1 &= \tfrac{1}{2h_a}(v_c - v_b) - h_a^2 v_3 \end{aligned} \tag{37}$$

reducing thus the total number of fundamental kinematic unknowns to 9 for the description of the three-layer assembly which will be further discretized along the longitudinal direction. These primary unknowns can be brought together in a unique vector as follows:

$$\mathbf{d}(x) = \langle u_b\ u_c\ v_b\ v_c\ \theta_b\ \theta_c\ u_2\ v_2\ v_3 \rangle^T \tag{38}$$

4.2. Numerical implementation

4.2.1. Weak formulation

The numerical discretization of the problem is further derived from the virtual work principle. The following equilibrium relation holds for any kinematically admissible displacement variation $\delta\mathbf{u}$:

$$\delta\mathcal{W}_{int}(\delta\mathbf{u}) + \delta\mathcal{W}_{ext}(\delta\mathbf{u}) = 0 \tag{39}$$

On one hand, the virtual work of the internal forces $\delta\mathcal{W}_{int}$ for the whole structure takes the following form:

$$\begin{aligned}
\delta\mathcal{W}_{int} &= -\textstyle\sum_{i=a,b,c}\int_{\Omega_i}\delta\boldsymbol{\varepsilon}_i^T\boldsymbol{\sigma}_i\mathrm{d}\Omega \\
&= -\int_{-L_s-L_a}^{-L_a}\left(\int_{-h_s}^{h_s}\delta\boldsymbol{\varepsilon}_c^T\boldsymbol{\sigma}_c\mathrm{d}y\right)\mathrm{d}x \\
&\quad -\int_{-L_a}^{L_a}\left(\int_{-h_s}^{h_s}\delta\boldsymbol{\varepsilon}_c^T\boldsymbol{\sigma}_c\mathrm{d}y + \int_{-h_s}^{h_s}\delta\boldsymbol{\varepsilon}_b^T\boldsymbol{\sigma}_b\mathrm{d}y + \int_{-h_a}^{h_a}\delta\boldsymbol{\varepsilon}_a^T\boldsymbol{\sigma}_a\mathrm{d}y\right)\mathrm{d}x \\
&\quad -\int_{L_a}^{L_a+L_s}\left(\int_{-h_s}^{h_s}\delta\boldsymbol{\varepsilon}_b^T\boldsymbol{\sigma}_b\mathrm{d}y\right)\mathrm{d}x
\end{aligned} \tag{40}$$

Let us focus again on the overlap zone and introduce the following vector of generalized displacements (where functions u_0, u_1, v_0 and v_1 and their derivatives have been discarded since, due to the continuity conditions, they represent auxiliary variables which depend on the key variables of Equation (38)):

$$\mathbf{q}(x) = \langle u_b\ u_c\ u_{b,x}\ \ u_{c,x}\ \ v_b\ v_c\ v_{b,x}\ \ v_{c,x}\ \ \theta_b\ \theta_c\ \theta_{b,x}\ \ \theta_{c,x}\ \ u_2\ u_{2,x}\ \ v_2\ v_{2,x}\ \ v_3\ v_{3,x}\rangle^T \tag{41}$$

and the matrices $\mathbf{H}_a$, $\mathbf{H}_b$ and $\mathbf{H}_c$ (whose non-zero components are reported in Appendix B) such that:

$$\boldsymbol{\varepsilon}_i = \mathbf{H}_i\mathbf{q} \qquad\qquad (i = a, b, c) \tag{42}$$

The internal virtual work within the three-layer region can then be rewritten in the following form:

$$\delta\mathcal{W}_{int} = -\int_{-L_a}^{L_a}\left(\int_{-h_s}^{h_s}\delta\mathbf{q}^T\mathbf{H}_c^T\mathbf{L}_s\mathbf{H}_c\mathbf{q}\mathrm{d}y + \int_{-h_s}^{h_s}\delta\mathbf{q}^T\mathbf{H}_b^T\mathbf{L}_s\mathbf{H}_b\mathbf{q}\mathrm{d}y + \int_{-h_a}^{h_a}\delta\mathbf{q}^T\mathbf{H}_a^T\boldsymbol{\sigma}_a\mathrm{d}y\right)\mathrm{d}x \tag{43}$$

Similar expressions can be written for the unbonded parts of the substrates by defining new vectors of generalized displacements $\mathbf{q}_b$ and $\mathbf{q}_c$, containing only the three displacement components (and their derivatives) related to the adherends b and c, respectively.

On the other hand, the external virtual work $\delta\mathcal{W}_{ext}$ relates to the external loads applied to the SLJ. The only applied forces that will be considered in the sequel are localized at the two ends of the SLJ, and $\delta\mathcal{W}_{ext}$ can thus be written as follows:

$$\delta\mathcal{W}_{ext} = \delta\mathbf{q}_c^T(-L_s - L_a)\boldsymbol{\Phi}_c + \delta\mathbf{q}_b^T(L_a + L_s)\boldsymbol{\Phi}_b \tag{44}$$

$\boldsymbol{\Phi}_b$ and $\boldsymbol{\Phi}_c$ represent vectors of generalized forces. In the present case of tensile forces, the first components of $\boldsymbol{\Phi}_b$ and $\boldsymbol{\Phi}_c$ (associated with the longitudinal displacements u_b and u_c) are equal to F and $-F$, respectively. All the remaining components are zero.

4.2.2. Finite element discretization

The problem is now discretized using 3-node isoparametric elements with quadratic shape functions.

Within a 1D given finite element e in the overlap region, all the components of vector $\mathbf{d}$ are interpolated in the same way, introducing the elementary nodal displacement vector $\mathbf{D}^e$ composed of the 27 degrees of freedom of the given element and the associated interpolation matrix $\mathbf{N}$ consisting of shape functions:

$$\mathbf{d} = \mathbf{N}\mathbf{D}^e \tag{45}$$

with $\mathbf{D}^e = \left\langle \mathbf{D}_1^{e^T}\ \mathbf{D}_2^{e^T}\ \mathbf{D}_3^{e^T} \right\rangle^T$, where $\mathbf{D}_i^e \triangleq \mathbf{d}(x_i) = \langle u_b\ u_c\ v_b\ v_c\ \theta_b\ \theta_c\ u_2\ v_2\ v_3 \rangle_i^T$ contains the 9 degrees of freedom of the i-th node of element e.

Finally, the generalized displacement vector $\mathbf{q}$ may be expressed in terms of $\mathbf{d}$ (by means of a transformation matrix $\mathbf{T}$ including differential operators) and subsequently in terms of $\mathbf{D}^e$ as follows:

$$\mathbf{q} = \mathbf{T}\mathbf{d} = \mathbf{T}\mathbf{N}\mathbf{D}^e \triangleq \mathbf{G}\mathbf{D}^e \tag{46}$$

According to all these definitions, Equation (43) can be rewritten in the following discretized form:

$$\delta\mathcal{W}_{int} = \sum_e \delta\mathcal{W}_{int}^e = -\sum_e \int_{-1}^{1} \delta\mathbf{D}^{e^T} \left(\int_{-h_s}^{h_s} \mathbf{B}_c^T \mathbf{L}_s \mathbf{B}_c \mathrm{d}y \mathbf{D}^e + \int_{-h_s}^{h_s} \mathbf{B}_b^T \mathbf{L}_s \mathbf{B}_b \mathrm{d}y \mathbf{D}^e + \int_{-h_a}^{h_a} \mathbf{B}_a^T \boldsymbol{\sigma}_a \mathrm{d}y \right) \frac{L_e}{2} \mathrm{d}\xi \tag{47}$$

where:

$$\mathbf{B}_i = \mathbf{H}_i \mathbf{G} \qquad (i = a, b, c) \tag{48}$$

It should be mentioned that the integrations with respect to the y-coordinate are performed analytically through the thickness of the adherends (introducing a shear correction factor of 5/6 in the resulting shear quantities, as for homogeneous beams, according to the Timoshenko beam theory), while numerical integrations using Gaussian quadratures are carried out through the thickness of the adhesive layer, as it involves more complex kinematics and, above all, possible material non-linearities. Besides, the integration over a real element is replaced by the integration over the reference element, by means of the following variable change: $dx = \frac{L_e}{2} d\xi$ (L_e being the elementary length). A numerical integration scheme (using also Gaussian points) is classically employed for the calculation of integrals in the longitudinal direction.

Equation (46) can also be truncated to the displacement components of adherend b or c, so as to express the generalized displacement vector in each separated substrate as a function of the corresponding displacement fields and finally in terms of the proper degrees of freedom (using the same interpolation functions for the considered components). Then, the total internal virtual work (40) can be expressed as in Equation (47), with supplementary terms which will not be further detailed, as they refer to classical Timoshenko beam finite elements. Likewise, the external virtual work can be expressed in terms of the appropriate degrees of freedom.

After assembling along the SLJ over all the finite elements (enriched three-layer elements for the overlap region and classical beam elements for the unbonded parts), one can express the discretized equilibrium equations in the following concise form:

$$\mathbf{R}(\mathbf{D}) = \mathbf{\Psi}(\mathbf{D}) - \mathbf{F} = \mathbf{0} \tag{49}$$

where $\mathbf{R}$ represents the residual vector, $\mathbf{\Psi}$ and $\mathbf{F}$ standing for the global internal and external force vectors, respectively, associated to the global nodal displacement vector $\mathbf{D}$.

4.2.3. Solution procedure

Owing to the elastoplastic constitutive law assumed for the adhesive material, the stress vector $\boldsymbol{\sigma}_a$ in Equation (47) cannot be linearly expressed in terms of the degrees of freedom. Consequently, the equation system (49) is non-linear and will be solved incrementally, using the iterative Newton-Raphson procedure. For each loading increment, at current iteration $i+1$, the nodal displacement vector is updated as follows:

$$\mathbf{D}^{(i+1)} = \mathbf{D}^{(i)} + \underbrace{\left(\left. \frac{\partial \mathbf{R}(\mathbf{D})}{\partial \mathbf{D}} \right|_{\mathbf{D}=\mathbf{D}^{(i)}} \right)^{-1}}_{\mathbf{K}_T^{-1}} \mathbf{R}(\mathbf{D}^{(i)}) \tag{50}$$

In Equation (50), $\mathbf{R}(\mathbf{D}^{(i)})$ represents the residual force vector at iteration i, which must converge towards zero. This iterative procedure requires the computation of the structural tangent stiffness matrix:

$$\mathbf{K}_T = \frac{\partial \mathbf{R}(\mathbf{D})}{\partial \mathbf{D}} = \frac{\partial \mathbf{\Psi}(\mathbf{D})}{\partial \mathbf{D}} \tag{51}$$

which depends on the consistent tangent operator, deriving itself from the local integration of the constitutive laws, among other things.

The derivation of internal forces within the overlap region necessitates numerical integration through the adhesive thickness and, at each Gaussian point, the stresses $\boldsymbol{\sigma}_a$ are evaluated by a local iterative integration procedure of the elastoplastic constitutive equations, using an implicit Euler scheme and a return mapping algorithm compliant with the assumed plane stress condition, as described in [21] and explained below.

The evolution laws (Equations (33) and (34)) are first discretized with respect to time:

$$\begin{aligned} (\boldsymbol{\varepsilon}_a^p)_{n+1} &= (\boldsymbol{\varepsilon}_a^p)_n + \Delta\Lambda \mathbf{P}(\boldsymbol{\sigma}_a)_{n+1} \\ p_{n+1} &= p_n + \Delta\Lambda \sqrt{\tfrac{2}{3}(\boldsymbol{\sigma}_a)_{n+1}^T \mathbf{P}(\boldsymbol{\sigma}_a)_{n+1}} \end{aligned} \tag{52}$$

Given the displacements (and thus the total deformation state $(\boldsymbol{\varepsilon}_a)_{n+1}$ at each integration point) at current time increment, the problem consists in updating the new stress and plastic strain states ($(\boldsymbol{\sigma}_a)_{n+1}$, $(\boldsymbol{\varepsilon}_a^p)_{n+1}$ and p_{n+1}) from the previous states (at time increment n) and determining the consistent tangent elastoplastic operator $(\mathbf{L}_a^{ep})_{n+1}$ at the same time. In a first step, a trial elastic prediction is performed as follows:

$$\begin{aligned} \boldsymbol{\sigma}_a^E &= \mathbf{L}_a \left((\boldsymbol{\varepsilon}_a)_{n+1} - (\boldsymbol{\varepsilon}_a^p)_n \right) \\ p^E &= p_n \end{aligned} \tag{53}$$

Either the yield criterion is verified ($f \leq 0$), in which case the updated stress state is the trial state, the plastic quantities are unchanged and the tangent operator is purely elastic, or a second step of plastic correction is needed. In the latter case, the increment of plastic multiplier $\Delta\Lambda$ is obtained first by solving the following yield condition (at time increment $n+1$), using a local Newton-Raphson iterative procedure:

$$f = \frac{1}{2}(\boldsymbol{\sigma}_a)_{n+1}^T \mathbf{P}(\boldsymbol{\sigma}_a)_{n+1} - \frac{1}{3}(\sigma_y^a + A(p_{n+1}))^2 \tag{54}$$

where:

$$\begin{cases} (\boldsymbol{\sigma}_a)_{n+1} = \Gamma(\Delta\Lambda)\mathbf{L}_a^{-1}\boldsymbol{\sigma}_a^E & \text{with: } \Gamma(\Delta\Lambda) = (\mathbf{L}_a^{-1} + \Delta\Lambda\mathbf{P})^{-1} \\ p_{n+1} = p_n + \Delta\Lambda\sqrt{\frac{2}{3}(\boldsymbol{\sigma}_a)_{n+1}^T \mathbf{P}(\boldsymbol{\sigma}_a)_{n+1}} \end{cases} \tag{55}$$

It then remains to update the plastic strain vector as in Equation (52), and the consistent tangent operator (to be used in the computation of the tangent stiffness matrix) can be finally expressed as a function of the consistency parameter $\Delta\Lambda$ [22]:

$$(\mathbf{L}_a^{ep})_{n+1} = \frac{\partial(\boldsymbol{\sigma}_a)_{n+1}}{\partial(\boldsymbol{\varepsilon}_a)_{n+1}} = \Gamma(\Delta\Lambda) - \frac{(\Gamma(\Delta\Lambda)\mathbf{P}(\boldsymbol{\sigma}_a)_{n+1})(\Gamma(\Delta\Lambda)\mathbf{P}(\boldsymbol{\sigma}_a)_{n+1})^T}{(\boldsymbol{\sigma}_a)_{n+1}^T \mathbf{P}^T \Gamma(\Delta\Lambda)\mathbf{P}(\boldsymbol{\sigma}_a)_{n+1} + \beta} \tag{56}$$

where:

$$\beta = \frac{2H_a}{3 - 2\Delta\Lambda H_a}(\boldsymbol{\sigma}_a)_{n+1}^T \mathbf{P}(\boldsymbol{\sigma}_a)_{n+1} \tag{57}$$

5. Numerical results and validation

5.1. Numerical models

The previous finite element formulation has been implemented in a home-made Matlab program. This code combines the use of 1D enriched three-layer elements, as originally developed in this study, and standard Timoshenko beam elements, and is thus devoted to the analysis of arbitrary assemblies of beams with possibly several bonded regions and arbitrary geometric and loading configurations. In this paper, it is used to analyze the mechanical response of a SLJ under tensile forces. The geometric and material configuration is the same as already used in the analytical part (see Tables 1 and 2). In addition to the elastic properties of the adhesive material, one must specify here the yield stress $\sigma_y^a = 12\ MPa$ and the hardening modulus $H_a = 100\ MPa$ to be used in case of plasticity. The boundary conditions are consistent with the ones already applied in the analytical solution and in the 2D numerical computations: the transverse displacements of both ends of the SLJ (namely $v_c(-L_s - L_a)$ and $v_b(L_a + L_s)$ are set to zero). After a short convergence analysis, a final mesh of 100 elements for the overlap zone and 50 elements for each unbonded substrate is retained in the subsequent computations involving the 1D finite element model. Besides, 5 Gaussian points are used both in the thickness direction of the adhesive layer and in the length of each 1D finite element for the numerical integration.

For validation purposes, 2D numerical finite element computations are performed again using Abaqus software, with the same modeling parameters as before, in both cases of an elastic and elastoplastic behavior of the adhesive material.

Again, a few parametric analyses have been performed in this study, which will not be presented in the current paper for conciseness purposes, since in all practical cases, similar significant features were observed and the same conclusions were drawn.

5.2. Elastic adhesive material

In elasticity, a tensile force of 5000 N is applied at both ends, as in the previous analytical study. For illustration purposes, the general deformed shape of the SLJ is displayed in Figure 5 (with a magnified deformation scale factor). Then, the different stresses are extrapolated all over the adhesive surface and plotted again along the centroid axis of the adhesive layer and at the upper interface between adhesive and substrate (see Figures 6 and 7).

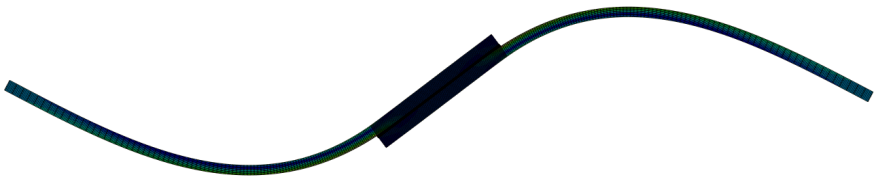

Figure 5: Deformed shape of the single-lap joint under tensile loading

The results show a perfect agreement between both simplified and standard models, particularly near the interfaces at the ends of the overlap region in the vicinity of singularities (where asymptotic curves are obtained). Again, contrary to classical analytical or even simplified numerical models in the literature, the present numerical tool allows one to evaluate the longitudinal stress through out the adhesive joint with a very good accuracy. This stress turns out to be non negligible when compared to the other stresses and its contribution to a given equivalent stress or failure criterion may not be incidental. For instance, along the centroid axis of the adhesive layer (see Figure 6), the maximum longitudinal stress attains one third and almost one half of the maximum peel and shear stresses, respectively. Along the upper interface (see Figure 7), the longitudinal stress is quite at the same level than the shear stress.

Many more configurations have been investigated in practice, for which similar results were obtained, with always a very good accordance between the 1D and 2D models, even in the case of non-symmetric SLJs which can be easily handled by the simplified numerical approach. No parametric analysis is thus performed here, for clarity purposes.

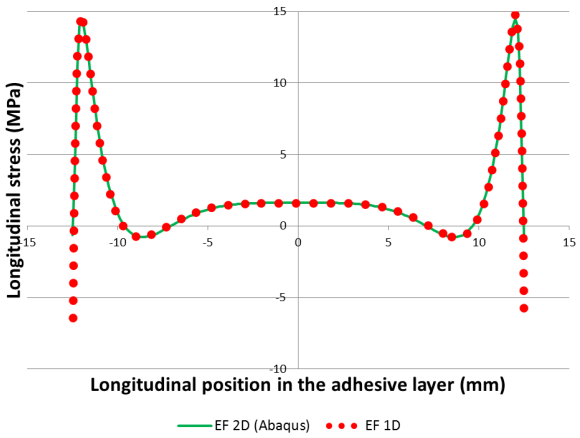

(a) Longitudinal stresses

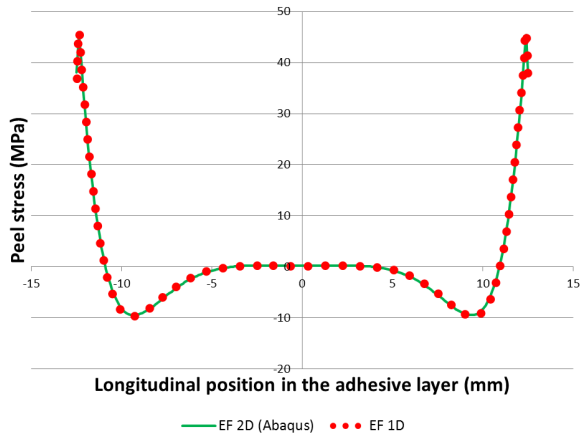

(b) Peel stresses

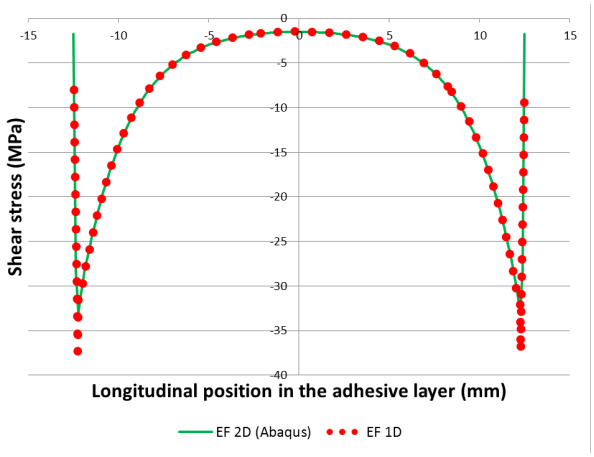

(c) Shear stresses

Figure 6: Comparison between 1D and 2D numerical stresses along the mid-line of the adhesive layer (elasticity)

5.3. Elastoplastic adhesive material

In a second phase, the adhesive material is supposed to be elastoplastic. A tensile force of 2500 N is applied at both ends, so as to partially plastify the adhesive joint. For illustration purposes, the different stress distributions are represented in Figure 8 with a particular focus on substrates, which allows one to identify the extreme zones where plasticity arises in the adhesive material.

Furthermore, the same curves are plotted as in the previous elastic case, namely the evolution of the different stress components along the adhesive length at the centroid axis of the adhesive layer and at the upper interface between adhesive and substrate (see Figures 9 and 10). A very good general agreement is still achieved between the two approaches, with almost the same accuracy as in the elastic case. It shows the relevance of the new 1D model, even in the more complex elastoplastic case, although the kinematics

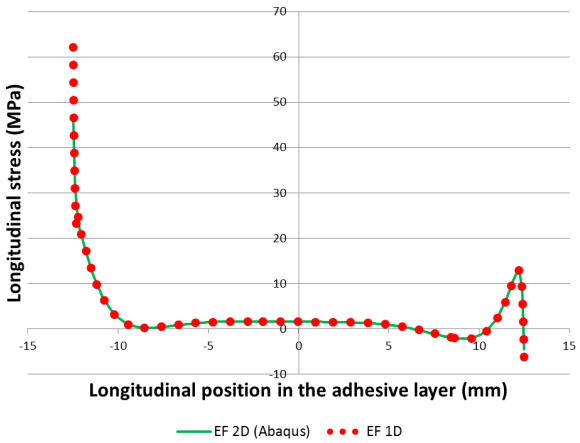

(a) Longitudinal stresses

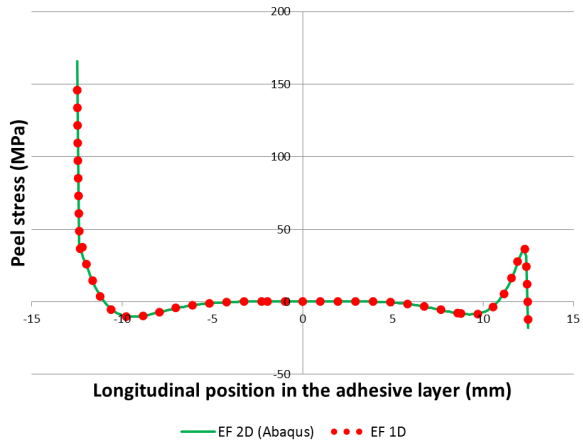

(b) Peel stresses

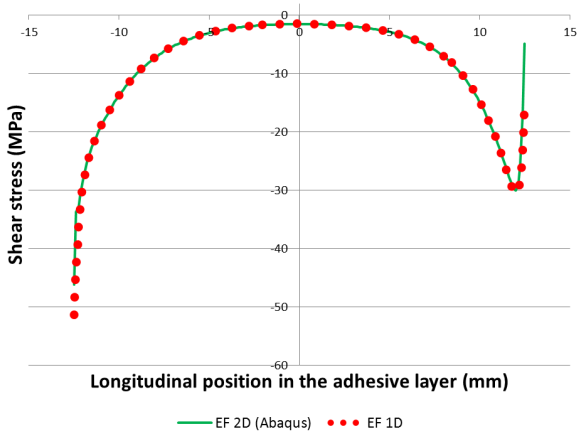

(c) Shear stresses

Figure 7: Comparison between 1D and 2D numerical stresses along the upper interface (elasticity)

were initially optimized in a pure linear elastic context. Let us mention that, again, the longitudinal stresses are of the same order of magnitude than the other ones.

All these results prove that the present numerical formulation is capable of capturing very accurately all the displacement fields and thus all the strain and stress fields inside the adhesive layer, contrary to more classical models with more approximate kinematics. In both elastic and elastoplastic cases, a perfect match is reached between 1D and 2D solutions throughout most of the surface. The concordance is just a little bit less pronounced, as soon as one gets closer to the ends of the adhesive zone. This numerical tool realizes thus a good compromise between accuracy, completeness and computational cost, and is likely to address many other geometric, material or loading configurations, with reasonable changes, and therefore to deal

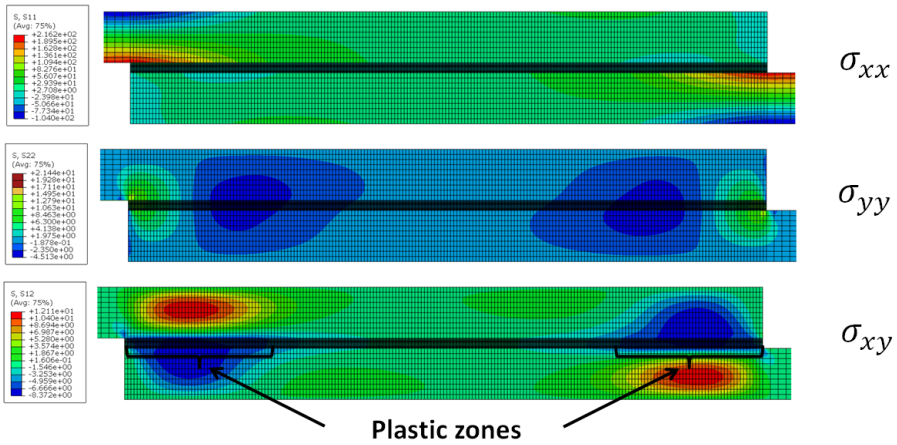

Figure 8: Stress components in the substrates for an elastoplastic adhesive material

efficiently with the mechanical analysis of any thin bonded structures.

6. Conclusions

The problem of a SLJ under tensile forces is investigated in this paper both analytically and numerically. The novelty of this work is based upon the choice of non-linear polynomial longitudinal and transverse displacement fields in the adhesive thickness direction, which allows one to describe with a good accuracy the peel and shear stresses as well as the longitudinal stresses all over the adhesive surface, in a 2D framework. The preliminary analytical study enables one to highlight the significance of non-linear terms in the polynomial developments of the kinematics, giving rise to an optimal choice of the polynomial orders. With such hypotheses, a 1D three-layer finite element is then developed. The two identical substrates are represented by elastic Timoshenko beams, including possible transverse shear effects in such a way that there is no particular restriction on their thickness, whereas the adhesive material is supposed to be elastoplastic. The problem of SLJ is then modeled using such enriched finite elements (displaying 9 degrees of freedom per node) in the overlap region and classical Timoshenko beam elements in the remaining parts. The longitudinal discretization of the displacement fields relies on quadratic shape functions, giving rise to 3-node elements. All the analytical and numerical computations are performed under the plane stress assumption, but can easily be generalized to the plane strain case, if needed.

The analytical and numerical results derived from this computationally efficient 1D formulation are compared to 2D finite element reference results obtained using Abaqus software, for validation purposes. The results are in very good agreement, in both cases of an elastic and elastoplastic adhesive material. These accurate results are obtained very efficiently thanks to a rigorous description of the deformation field in the adhesive layer, in both present analytical and numerical modeling approaches. The stress distributions are

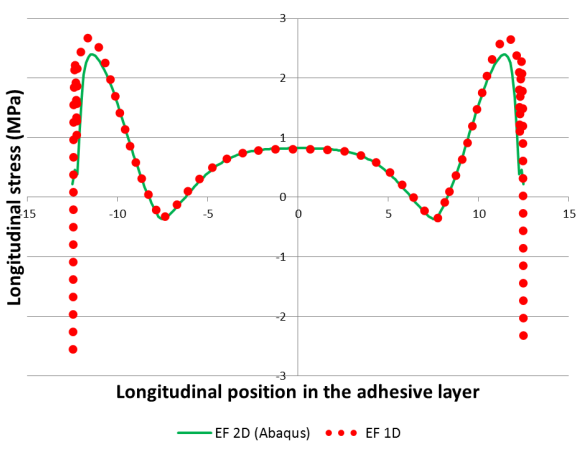

(a) Longitudinal stresses

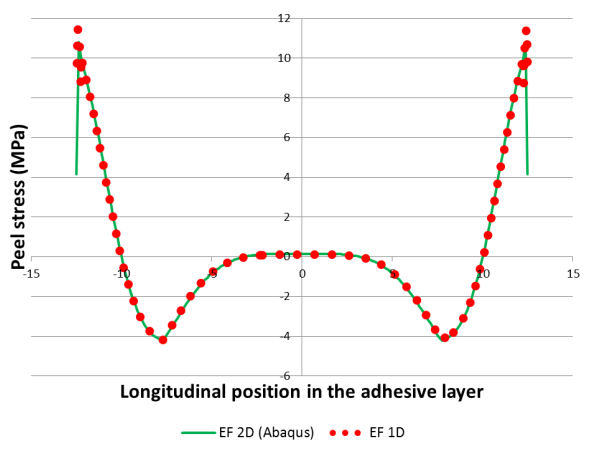

(b) Peel stresses

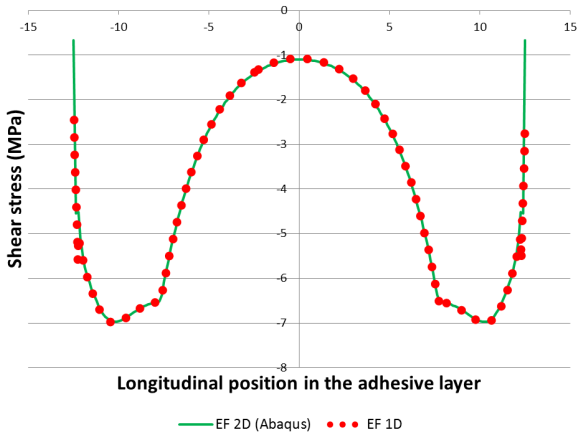

(c) Shear stresses

Figure 9: Comparison between 1D and 2D numerical stresses along the mid-line of the adhesive layer (elastoplasticity)

particularly reproduced in a robust and efficient way with a very good accuracy (once the appropriate order of kinematics is used), even in the vicinity of singularities, near the ends of the interfaces between adhesive and adherends. All these results show the utmost importance of non-linear terms in the displacement fields, which are crucial for an appropriate description of the stress variations through the thickness. Regarding the computational cost, the present 1D finite element is undoubtedly more time-consuming than other simple models based on spring distributions or beam formulations for the representation of the adhesive layer. However, it remains far computationally-inexpensive when compared to full 2D finite elements.

This 1D finite element model is prone to be used in more general configurations with different geometries and loading/boundary conditions, as long as beam-columns are involved and a three-layer representation (substrate/adhesive/substrate) for the overlap regions is appropriate. Such a model can also be extrapo-

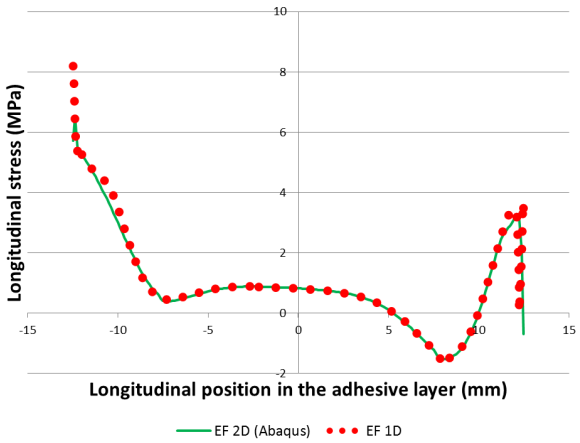

(a) Longitudinal stresses

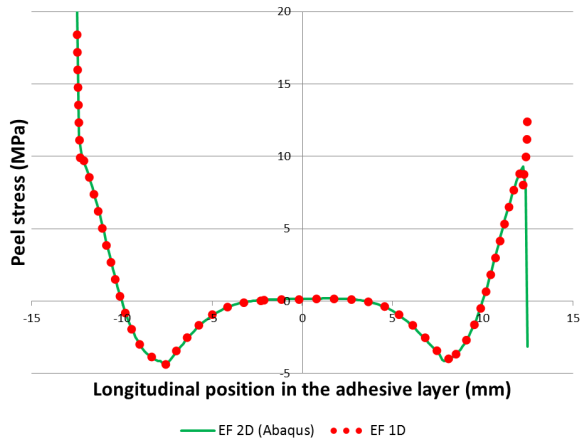

(b) Peel stresses

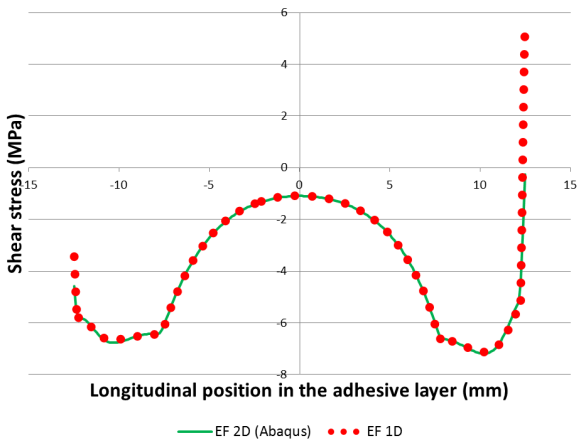

(c) Shear stresses

Figure 10: Comparison between 1D and 2D numerical stresses along the upper interface (elastoplasticity)

lated to other constitutive laws. The generalization of the present finite element to the context of finite transformations is part of the short-term objectives. The introduction of inertial effects and/or geometric non-linearities will make it possible to deal further with (non-linear) dynamic problems or instabilities, respectively. What is more, special attention should be paid to the mechanical (and failure) behavior of the interfaces between adherends and adhesive, introducing appropriate cohesive models. More generally, the present model enables one to investigate further even the cohesive failure of adhesive joints in a straightforward and rigorous integrated way, considering the adhesive layer like a thick enriched cohesive zone.

Acknowledgements

The authors are grateful to the Brittany Regional Council (France) for its financial support (Contract

no. SAD17004).

References

[1] Volkersen, O., Die Niektraftverteilung in Zugbeanspruchten mit konstanten Laschenquerschritten, *Luftfahrtforschung* **15** (1938) 41–47.

[2] Goland, M. and Reissner, E., Stresses in cemented joints, *Journal of Applied Mechanics* **11** (1944) A17–A27.

[3] Mortensen, F. and Thomsen, O.T., Analysis of adhesive bonded joints: a unified approach, *Composites Science and Technology* **62** Issues 7-8 (2002) 1011–1031.

[4] Stein, N., Felger, J. and Becker, W., Analytical models for functionally graded adhesive single lap joints: A comparative study, *International Journal of Adhesion and Adhesives* **76** (2017) 70–82.

[5] Da Silva, L.F.M., Das Neves, P.J.C., Adams, R.D. and Spelt, J.K., Analytical models of adhesively bonded joints – Part I: Literature survey, *International Journal of Adhesion and Adhesives* **29** Issue 3 (2009) 319–330.

[6] Allman, D.J., A theory for elastic stresses in adhesive bonded lap joints, *Quarterly Journal of Mechanics and Applied Mathematics* **30** (1977) 415–436.

[7] Zhao, B., Lu, Z.H. and Lu, Y.N., Closed-form solutions for elastic stress–strain analysis in unbalanced adhesive single-lap joints considering adherend deformations and bond thickness, *International Journal of Adhesion and Adhesives* **31** Issue 6 (2011) 434–445.

[8] Jiang, Z., Wan, S., Zhong, Z., Li, P., Li, S. and He, Y., Two-dimensional analysis for an adhesively bonded composite single-lap joint based on flexible interface theory, *Journal of Adhesion Science and Technology* **29** Issue 22 (2015) 2408–2432.

[9] Jiang, Z., Wan, S., Keller, T. and Vassilopoulos, A.P., Two-dimensional analytical stress distribution model for unbalanced FRP composite single-lap joints, *European Journal of Mechanics - A/Solids* **66** (2017) 341–355.

[10] Jiang, Z., Wan, S. and Song, A., An alternative solution for the edge moment factors of the unbalanced adhesive single-lap joint in tension, *International Journal of Adhesion and Adhesives* **75** (2017) 1–16.

[11] Cognard, J.Y., Créac'hcadec, R. and Maurice, J., Numerical analysis of the stress distribution in single-lap shear tests under elastic assumption – Application to the optimisation of the mechanical behaviour, *International Journal of Adhesion and Adhesives* **31** Issue 7 (2011) 715–724.

[12] Gonçalves, J.P.M., De Moura, M.F.S.F. and De Castro, P.M.S.T., A three-dimensional finite element model for stress analysis of adhesive joints, *International Journal of Adhesion and Adhesives* **22** Issue 5 (2002) 357–365.

[13] Lin, C.C. and Lin, Y.S., A finite element model of single-lap adhesive joints, *International Journal of Solids and Structures* **30** Issue 12 (1993) 1679–1692.

[14] Tong, L. and Sun, X., Adhesive elements for stress analysis of bonded patch to curved thin-walled structures, *Computational Mechanics* **30** (2003) 143–154.

[15] Paroissien, E., Gaubert, F., Da Veiga, A. and Lachaud, F., Elasto-plastic analysis of bonded joints with macro-elements, *Journal of Adhesion Science and Technology* **27** Issue 13 (2013) 1464–1498.

[16] Stapleton, S.E., Waas, A.M. and Bednarcyk, B.A., Modeling progressive failure of bonded joints using a single joint finite element, *AIAA Journal* **49** Issue 8 (2011) 1740–1749.

[17] Stapleton, S.E., Waas, A.M. and Arnold, S.M., Functionally graded adhesives for composite joints, *International Journal of Adhesion and Adhesives* **35** (2012) 36–49.

[18] Stapleton, S.E., Pineda, E.J., Gries, T. and Waas, A.M., Adaptive shape functions and internal mesh adaptation for modeling progressive failure in adhesively bonded joints, *International Journal of Solids and Structures* **51** Issue 18 (2014) 3252–3264.

[19] Tsai, M.Y., Oplinger, D.W. and Morton, J., Improved theoretical solutions for adhesive lap joints, *International Journal of Solids and Structures* **35** Issue 12 (1998) 1163–1185.

[20] Stein, N., Mardani, H. and Becker, W., An efficient analysis model for functionally graded adhesive single lap joints, *International Journal of Adhesion and Adhesives* **70** (2016) 117–125.

[21] Simo, J.C. and Taylor, R.L., A return mapping algorithm for plane stress elastoplasticity, *International Journal for Numerical Methods in Engineering* **22** Issue 3 (1986) 649–670.

[22] Simo, J.C. and Taylor, R.L., Consistent tangent operators for rate-independent elastoplasticity, *Computer Methods in Applied Mechanics and Engineering* **48** Issue 1 (1985) 101–118.

Appendix A. Analytical expressions in the case of second-order kinematics in the adhesive layer

The analytical formulation of the problem is recalled here, but considering henceforth second-order kinematics in the adhesive layer. The same notations are used as before.

The kinematics are thus unchanged in the adherends and take the new following quadratic expressions in the adhesive:

$$\mathbf{u}_a(x,y) = \left| \begin{array}{l} u_0(x) + u_1(x)\ y + u_2(x)\ y^2 \\ v_0(x) + v_1(x)\ y + v_2(x)\ y^2 \end{array} \right. \tag{A.1}$$

The corresponding strain and stress tensors become then:

$$\begin{aligned} \boldsymbol{\varepsilon}_a &= \left\{ \begin{array}{c} \varepsilon^a_{xx} \\ \varepsilon^a_{yy} \\ 2\varepsilon^a_{xy} \end{array} \right\} = \left\{ \begin{array}{c} u_{0,x} + u_{1,x}\, y + u_{2,x}\, y^2 \\ v_1 + 2v_2 y \\ u_1 + 2u_2 y + v_{0,x} + v_{1,x}\, y + v_{2,x}\, y^2 \end{array} \right\} \\ \boldsymbol{\sigma}_a &= \left\{ \begin{array}{c} \sigma^a_{xx} \\ \sigma^a_{yy} \\ \sigma^a_{xy} \end{array} \right\} = \left\{ \begin{array}{c} (\lambda'_a + 2\mu_a)(u_{0,x} + u_{1,x}\, y + u_{2,x}\, y^2) + \lambda'_a(v_1 + 2v_2 y) \\ \lambda'_a(u_{0,x} + u_{1,x}\, y + u_{2,x}\, y^2) + (\lambda'_a + 2\mu_a)(v_1 + 2v_2 y) \\ \mu_a(u_1 + 2u_2 y + v_{0,x} + v_{1,x}\, y + v_{2,x}\, y^2) \end{array} \right\} \end{aligned} \tag{A.2}$$

The displacement continuity conditions at the interfaces between adhesive and substrates lead here to the following relations:

$$\forall x \in]-L_a, L_a[, \qquad \begin{array}{l} u_b = h_s\theta_b + u_0 - h_a u_1 + h_a^2 u_2 \\ v_b = v_0 - h_a v_1 + h_a^2 v_2 \\ u_c = -h_s\theta_c + u_0 + h_a u_1 + h_a^2 u_2 \\ v_c = v_0 + h_a v_1 + h_a^2 v_2 \end{array} \tag{A.3}$$

Finally, the differential equilibrium equations are obtained:

- $\forall x \in]-L_s - L_a, -L_a[$:

$$\begin{array}{l} 2E_s h_s u^l_{c,xx} = 0 \\ 2kG_s h_s(v^l_{c,xx} - \theta^l_{c,x}) = 0 \\ \frac{2E_s h_s^3}{3}\theta^l_{c,xx} + 2kG_s h_s(v^l_{c,x} - \theta^l_c) = 0 \end{array} \tag{A.4}$$

- $\forall x \in]-L_a, L_a[$:

$$
\begin{aligned}
&\tfrac{2E_s h_s^3}{3}\theta_{b,xx} + 2E_s h_s^2(h_s\theta_{b,xx} + u_{0,xx} - h_a u_{1,xx} + h_a^2 u_{2,xx}) + 2kG_s h_s(-\theta_b + v_{0,x} - h_a v_{1,x} + h_a^2 v_{2,x}) = 0\\
&\tfrac{2E_s h_s^3}{3}\theta_{c,xx} - 2E_s h_s^2(-h_s\theta_{c,xx} + u_{0,xx} + h_a u_{1,xx} + h_a^2 u_{2,xx}) + 2kG_s h_s(-\theta_c + v_{0,x} + h_a v_{1,x} + h_a^2 v_{2,x}) = 0\\
&(\lambda_a' + 2\mu_a)(2h_a u_{0,xx} + \tfrac{2h_a^3}{3}u_{2,xx}) + 2\lambda_a' h_a v_{1,x} + 2E_s h_s(h_s\theta_{b,xx} - h_s\theta_{c,xx} + 2u_{0,xx} + 2h_a^2 u_{2,xx}) = 0\\
&(\lambda_a' + 2\mu_a)\tfrac{2h_a^3}{3}u_{1,xx} + \lambda_a'\tfrac{4h_a^3}{3}v_{2,x} - \mu_a(2h_a u_1 + 2h_a v_{0,x} + \tfrac{2h_a^3}{3}v_{2,x})\\
&+2E_s h_s h_a(-h_s\theta_{b,xx} - h_s\theta_{c,xx} + 2h_a u_{1,xx}) = 0\\
&(\lambda_a' + 2\mu_a)(\tfrac{2h_a^3}{3}u_{0,xx} + \tfrac{2h_a^5}{5}u_{2,xx}) + \lambda_a'\tfrac{2h_a^3}{3}v_{1,x} - \mu_a(\tfrac{8h_a^3}{3}u_2 + \tfrac{4h_a^3}{3}v_{1,x})\\
&+2E_s h_s h_a^2(h_s\theta_{b,xx} - h_s\theta_{c,xx} + 2u_{0,xx} + 2h_a^2 u_{2,xx}) = 0\\
&\mu_a(2h_a u_{1,x} + 2h_a v_{0,xx} + \tfrac{2h_a^3}{3}v_{2,xx}) + 2kG_s h_s(-\theta_{b,x} - \theta_{c,x} + 2v_{0,xx} + 2h_a^2 v_{2,xx}) = 0\\
&\lambda_a'(2h_a u_{0,x} + \tfrac{2h_a^3}{3}u_{2,x}) + 2(\lambda_a' + 2\mu_a)h_a v_1 - \mu_a(\tfrac{4h_a^3}{3}u_{2,x} + \tfrac{2h_a^3}{3}v_{1,xx})\\
&-2kG_s h_s h_a(\theta_{b,x} - \theta_{c,x} + 2h_a v_{1,xx}) = 0\\
&\lambda_a'\tfrac{4h_a^3}{3}u_{1,x} + (\lambda_a' + 2\mu_a)\tfrac{8h_a^3}{3}v_2 - \mu_a(\tfrac{2h_a^3}{3}u_{1,x} + \tfrac{2h_a^3}{3}v_{0,xx} + \tfrac{2h_a^5}{5}v_{2,xx})\\
&-2kG_s h_s h_a^2(-\theta_{b,x} - \theta_{c,x} + 2v_{0,xx} + 2h_a^2 v_{2,xx}) = 0
\end{aligned}
\tag{A.5}
$$

- $\forall x \in]L_a, L_a + L_s[$:

$$
\begin{aligned}
&2E_s h_s u_{b,xx}^r = 0\\
&2kG_s h_s(v_{b,xx}^r - \theta_{b,x}^r) = 0\\
&\tfrac{2E_s h_s^3}{3}\theta_{b,xx}^r + 2kG_s h_s(v_{b,x}^r - \theta_b^r) = 0
\end{aligned}
\tag{A.6}
$$

together with the continuity and boundary conditions, which write:

- For $x = -L_s - L_a$:

$$
\begin{aligned}
&2E_s h_s t u_{c,x}^l - F = 0\\
&v_c^l = 0\\
&\tfrac{2E_s h_s^3}{3}\theta_{c,x}^l = 0
\end{aligned}
\tag{A.7}
$$

- For $x = -L_a$:

$$
\begin{aligned}
&u_c^l = -h_s\theta_c + u_0 + h_a u_1 + h_a^2 u_2\\
&v_c^l = v_0 + h_a v_1 + h_a^2 v_2\\
&\theta_c^l = \theta_c
\end{aligned}
\tag{A.8}
$$

$$
\begin{aligned}
&\tfrac{2E_s h_s^3}{3}(\theta_{c,x}^l - 4\theta_{c,x}) + 2E_s h_s^2(-u_{c,x}^l + u_{0,x} + h_a u_{1,x} + h_a^2 u_{2,x}) = 0\\
&\tfrac{8E_s h_s^3}{3}\theta_{b,x} + 2E_s h_s^2(u_{0,x} - h_a u_{1,x} + h_a^2 u_{2,x}) = 0\\
&(\lambda_a' + 2\mu_a)(2h_a u_{0,x} + \tfrac{2h_a^3}{3}u_{2,x}) + 2\lambda_a' h_a v_1 + 2E_s h_s(h_s\theta_{b,x} - h_s\theta_{c,x} - u_{c,x}^l + 2u_{0,x} + 2h_a^2 u_{2,x}) = 0\\
&(\lambda_a' + 2\mu_a)\tfrac{2h_a^3}{3}u_{1,x} + \lambda_a'\tfrac{4h_a^3}{3}v_2 + 2E_s h_s h_a(-h_s\theta_{b,x} - h_s\theta_{c,x} - u_{c,x}^l + 2h_a u_{1,x}) = 0\\
&(\lambda_a' + 2\mu_a)(\tfrac{2h_a^3}{3}u_{0,x} + \tfrac{2h_a^5}{5}u_{2,x}) + \lambda_a'\tfrac{2h_a^3}{3}v_1 + 2E_s h_s h_a^2(h_s\theta_{b,x} - h_s\theta_{c,x} - u_{c,x}^l + 2u_{0,x} + 2h_a^2 u_{2,x}) = 0\\
&\mu_a(2h_a u_1 + 2h_a v_{0,x} + \tfrac{2h_a^3}{3}v_{2,x}) + 2kG_s h_s(-\theta_b - \theta_c + \theta_c^l - v_{c,x}^l + 2v_{0,x} + 2h_a^2 v_{2,x}) = 0\\
&\mu_a(\tfrac{4h_a^3}{3}u_2 + \tfrac{2h_a^3}{3}v_{1,x}) + 2kG_s h_s h_a(\theta_b - \theta_c + \theta_c^l - v_{c,x}^l + 2h_a v_{1,x}) = 0\\
&\mu_a(\tfrac{2h_a^3}{3}u_1 + \tfrac{2h_a^3}{3}v_{0,x} + \tfrac{2h_a^5}{5}v_{2,x}) + 2kG_s h_s h_a^2(-\theta_b - \theta_c + \theta_c^l - v_{c,x}^l + 2v_{0,x} + 2h_a^2 v_{2,x}) = 0
\end{aligned}
\tag{A.9}
$$

- For $x = L_a$:

$$
\begin{aligned}
u_b^r &= h_s\theta_b + u_0 - h_a u_1 + h_a^2 u_2\\
v_b^r &= v_0 - h_a v_1 + h_a^2 v_2\\
\theta_b^r &= \theta_b
\end{aligned}
\tag{A.10}
$$

$$
\begin{aligned}
&\tfrac{2E_s h_s^3}{3}(4\theta_{b,x} - \theta_{b,x}^r) + 2E_s h_s^2(-u_{b,x}^r + u_{0,x} - h_a u_{1,x} + h_a^2 u_{2,x}) = 0\\
&\tfrac{8E_s h_s^3}{3}\theta_{c,x} - 2E_s h_s^2(u_{0,x} + h_a u_{1,x} + h_a^2 u_{2,x}) = 0\\
&(\lambda_a' + 2\mu_a)(2h_a u_{0,x} + \tfrac{2h_a^3}{3}u_{2,x}) + 2\lambda_a' h_a v_1 + 2E_s h_s(h_s\theta_{b,x} - h_s\theta_{c,x} - u_{b,x}^r + 2u_{0,x} + 2h_a^2 u_{2,x}) = 0\\
&(\lambda_a' + 2\mu_a)\tfrac{2h_a^3}{3}u_{1,x} + \lambda_a'\tfrac{4h_a^3}{3}v_2 + 2E_s h_s h_a(-h_s\theta_{b,x} - h_s\theta_{c,x} + u_{b,x}^r + 2h_a u_{1,x}) = 0\\
&(\lambda_a' + 2\mu_a)(\tfrac{2h_a^3}{3}u_{0,x} + \tfrac{2h_a^5}{5}u_{2,x}) + \lambda_a'\tfrac{2h_a^3}{3}v_1 + 2E_s h_s h_a^2(h_s\theta_{b,x} - h_s\theta_{c,x} - u_{b,x}^r + 2u_{0,x} + 2h_a^2 u_{2,x}) = 0\\
&\mu_a(2h_a u_1 + 2h_a v_{0,x} + \tfrac{2h_a^3}{3}v_{2,x}) + 2kG_s h_s(-\theta_b - \theta_c + \theta_b^r - v_{b,x}^r + 2v_{0,x} + 2h_a^2 v_{2,x}) = 0\\
&\mu_a(\tfrac{4h_a^3}{3}u_2 + \tfrac{2h_a^3}{3}v_{1,x}) + 2kG_s h_s h_a(\theta_b - \theta_c - \theta_b^r + v_{b,x}^r + 2h_a v_{1,x}) = 0\\
&\mu_a(\tfrac{2h_a^3}{3}u_1 + \tfrac{2h_a^3}{3}v_{0,x} + \tfrac{2h_a^5}{5}v_{2,x}) + 2kG_s h_s h_a^2(-\theta_b - \theta_c + \theta_b^r - v_{b,x}^r + 2v_{0,x} + 2h_a^2 v_{2,x}) = 0
\end{aligned}
\tag{A.11}
$$

- For $x = L_a + L_s$:

$$
\begin{aligned}
&2E_s h_s t u_{b,x}^r - F = 0\\
&v_b^r = 0\\
&\tfrac{2E_s h_s^3}{3}\theta_{b,x}^r = 0
\end{aligned}
\tag{A.12}
$$

The solution procedure is similar to that already presented in the paper, but the expressions are here too cumbersome to be further specified.

Appendix B. Useful matrices

In the framework of small transformations, $\mathbf{H}_a$, $\mathbf{H}_b$ and $\mathbf{H}_c$ are constant matrices of $\mathbb{R}^{3\times 18}$, whose non-zero components are:

$$\begin{aligned}
&H_a(1,3) = \tfrac{1}{2}\left(1 - \tfrac{y}{h_a}\right)\\
&H_a(1,4) = \tfrac{1}{2}\left(1 + \tfrac{y}{h_a}\right)\\
&H_a(1,11) = -\tfrac{h_s}{2}\left(1 - \tfrac{y}{h_a}\right)\\
&H_a(1,12) = \tfrac{h_s}{2}\left(1 + \tfrac{y}{h_a}\right)\\
&H_a(1,14) = y^2 - h_a^2\\
&H_a(2,5) = -\tfrac{1}{2h_a}\\
&H_a(2,6) = \tfrac{1}{2h_a}\\
&H_a(2,15) = 2y\\
&H_a(2,17) = 3y^2 - h_a^2\\
&H_a(3,1) = -\tfrac{1}{2h_a}\\
&H_a(3,2) = \tfrac{1}{2h_a}\\
&H_a(3,7) = \tfrac{1}{2}\left(1 - \tfrac{y}{h_a}\right)\\
&H_a(3,8) = \tfrac{1}{2}\left(1 + \tfrac{y}{h_a}\right)\\
&H_a(3,9) = \tfrac{h_s}{2h_a}\\
&H_a(3,10) = \tfrac{h_s}{2h_a}\\
&H_a(3,13) = 2y\\
&H_a(3,16) = y^2 - h_a^2\\
&H_a(3,18) = y(y^2 - h_a^2)
\end{aligned} \tag{B.1}$$

$$\begin{aligned}
&H_b(1,3) = 1\\
&H_b(1,11) = -y\\
&H_b(3,7) = 1\\
&H_b(3,9) = -1
\end{aligned} \tag{B.2}$$

$$\begin{aligned}
&H_c(1,4) = 1\\
&H_c(1,12) = -y\\
&H_c(3,8) = 1\\
&H_c(3,10) = -1
\end{aligned} \tag{B.3}$$